

Climatic changes associated with a global “2°C-stabilization” scenario simulated by the ECHAM5/MPI-OM coupled climate model

Wilhelm May

Received: 8 September 2006 / Accepted: 4 December 2007 / Published online: 8 January 2008
© Springer-Verlag 2007

Abstract In this study, concentrations of the well-mixed greenhouse gases as well as the anthropogenic sulphate aerosol load and stratospheric ozone concentrations are prescribed to the ECHAM5/MPI-OM coupled climate model so that the simulated global warming does not exceed 2°C relative to pre-industrial times. The climatic changes associated with this so-called “2°C-stabilization” scenario are assessed in further detail, considering a variety of meteorological and oceanic variables. The climatic changes associated with such a relatively weak climate forcing supplement the recently published fourth assessment report by the IPCC in that such a stabilization scenario can only be achieved by mitigation initiatives. Also, the impact of the anthropogenic sulphate aerosol load and stratospheric ozone concentrations on the simulated climatic changes is investigated. For this particular climate model, the 2°C-stabilization scenario is characterized by the following atmospheric concentrations of the well-mixed greenhouse gases: 418 ppm (CO₂), 2,026 ppb (CH₄), and 331 ppb (N₂O), 786 ppt (CFC-11) and 486 ppt (CFC-12), respectively. These greenhouse gas concentrations correspond to those for 2020 according to the SRES A1B scenario. At the same time, the anthropogenic sulphate aerosol load and stratospheric ozone concentrations are changed to the level in 2100 (again, according to the SRES A1B scenario), with a global anthropogenic sulphur dioxide emission of 28 TgS/year leading to a global anthropogenic sulphate aerosol load of 0.23 TgS. The future changes in climate associated with the 2°C-stabilization scenario show many of the typical

features of other climate change scenarios, including those associated with stronger climatic forcings. That are a pronounced warming, particularly at high latitudes accompanied by a marked reduction of the sea-ice cover, a substantial increase in precipitation in the tropics as well as at mid- and high latitudes in both hemispheres but a marked reduction in the subtropics, a significant strengthening of the meridional temperature gradient between the tropical upper troposphere and the lower stratosphere in the extratropics accompanied by a pronounced intensification of the westerly winds in the lower stratosphere, and a strengthening of the westerly winds in the Southern Hemisphere extratropics throughout the troposphere. The magnitudes of these changes, however, are somewhat weaker than for the scenarios associated with stronger global warming due to stronger climatic forcings, such as the SRES A1B scenario. Some of the climatic changes associated with the 2°C-stabilization are relatively strong with respect to the magnitude of the simulated global warming, i.e., the pronounced warming and sea-ice reduction in the Arctic region, the strengthening of the meridional temperature gradient at the northern high latitudes and the general increase in precipitation. Other climatic changes, i.e., the El Niño like warming pattern in the tropical Pacific Ocean and the corresponding changes in the distribution of precipitation in the tropics and in the Southern Oscillation, are not as markedly pronounced as for the scenarios with a stronger global warming. A higher anthropogenic sulphate aerosol load (for 2030 as compared to the level in 2100 according to the SRES A1B scenario) generally weakens the future changes in climate, particularly for precipitation. The most pronounced effects occur in the Northern Hemisphere and in the tropics, where also the main sources of anthropogenic sulphate aerosols are located.

W. May (✉)
Danish Climate Centre, Danish Meteorological Institute,
Lyngbyvej 100, 2100 Copenhagen, Denmark
e-mail: wm@dmi.dk

1 Introduction

The objective of Article 2 of the United Nations Framework Convention on Climate Change (UNFCCC) formulated in 1992 is “to achieve stabilization of greenhouse gas concentrations in the atmosphere that would prevent dangerous anthropogenic interference with the climate system” (United Nations 1992). The convention further suggests that “such a level should be achieved within a time frame sufficient to allow ecosystems to adapt naturally to climate change, to ensure that food production is not threatened, and to enable economic development to proceed in a sustainable manner”. In accordance with this, the European Council adopted in 1996 a climate target reading as “the Council believes that the global average temperatures should not exceed 2° above pre-industrial level and that therefore concentration levels lower than 550 ppm CO₂ should guide global limitation and reduction efforts”. This so-called “EU-target” has been reaffirmed by the EU on a number of occasions, such as in 2002 by the Council of the Ministers for the Environment in the European Union, in 2004 again by the European Council and, most recently, in 2005 as an European Union Presidency Conclusion. Herein, the European Council also emphasises the need for “developing a medium and long-term EU strategy to combat climate change, consistent with the 2°C objective.”

But even an increase in the global mean temperature by 2°C can have wide-reaching adverse effects. An increase in the global mean temperature of about 2°C may cause a warming of about 2.7°C in the area around Greenland, possibly triggering the loss of the Greenland ice-sheet (Huybrechts et al. 1991; Gregory et al. 2004a, b). This loss would cause a global sea-level rise of 7 m over the next 1,000 years or more (Gregory et al. 2004a, b). Also, unique ecosystems such as coral reefs and ecosystems in the Arctic or mountain regions, which have been under increasing pressure, may be severely damaged by a global mean temperature increase of 2°C (e.g., Smith et al. 2001; ACIA 2005). Potentially positive feedbacks with the carbon cycle are increasingly likely with warmer temperatures (e.g., Friedlingstein et al. 2003; Jones et al. 2003a, b), further enhancing the anthropogenic increase in the global mean temperature. Potentially large but very uncertain methane releases might occur from thawing permafrost or ocean methane hydrates (Archer et al. 2004; Buffett and Archer 2004), again amplifying the global mean temperature increase.

In February 2005, an international symposium on “Avoiding Dangerous Climate Change” took place in Exeter, UK. Important issues of “dangerous” climate change were addressed, such as vulnerabilities of the climate system (and critical thresholds), vulnerabilities for

ecosystems and biodiversity, and vulnerabilities for water resources, agriculture and food as well as climate change impacts in various sensitive regions of the globe (Schellinghuber et al. 2006). Also, possible emission pathways to reach stabilization of the greenhouse gas concentrations at a level that could prevent dangerous climate change were discussed as well as technological options to realize these pathways.

Meinshausen (2006) addressed, for instance, the question of how low the greenhouse gas concentrations need to peak or stabilize at for not exceeding the EU-target of a maximum global mean temperature increase of 2°C. On the basis of a number of published climate sensitivities, he concluded that the probability for staying below a warming of 2°C at equilibrium is “likely” or “very likely” (according to the terminology of probabilities adopted by the Intergovernmental Panel on Climate Change; “IPCC”) at 400 ppm equivalent CO₂, while at 475 ppm the probability is at “medium likelihood” or “unlikely”. At 550 ppm equivalent CO₂, on the other hand, the risk of overshooting the EU-target is 63% and, assuming a climate sensitivity range consistent with the conventional range of 1.5–4.5°C used by the IPCC (Wigley and Raper 2001), the risk of overshooting 4°C as the global mean temperature increase is still 9%. However, assuming the more recently published probability density function (“PDF”) of climate sensitivity by Murphy et al. (2004), the risk of overshooting 4°C is as high as 25%. It was also found that if the equivalent CO₂ concentration temporarily overshoot the 400 ppm stabilization level by 75 ppm, the probability of keeping the future warming below 2°C decreases by 10–20%, depending on the rate at which the greenhouse gas concentrations are reduced after the peaking. However, the overshooting of such low stabilization levels might be necessary, given that a peaking at 475 ppm equivalent CO₂ is already asking for substantial emission reductions in the coming 2–3 decades.

Den Elzen and Meinshausen (2006) analyzed possible emission pathways including several greenhouse gases as well as the effects of aerosols for meeting the EU-target. They found that in order to reach the 400 ppm equivalent CO₂ stabilization level proposed by Meinshausen (2006) the global emissions should peak around the year 2015 in order to avoid global reduction rates exceeding 2.5% per year and should be reduced by as much as 40–50% in 2050 compared to the levels in 1990. Brasseur and Roeckner (2005), investigating the impact of improved air quality on the future evolution of climate, found that the stabilization of the sulphate aerosol load has such a pronounced effect on global warming that it has to be considered in strategies aiming to maintain the global warming below a certain threshold.

Meinshausen (2006) based his computations on a formula for the radiative forcing caused by increased CO₂ concentrations by Ramaswamy et al. (2001). He obtains the warming in equilibrium associated with a certain stabilized (equivalent) CO₂ concentration with respect to pre-industrial times by combining the corresponding radiative forcing with a measure of the climate sensitivity, i.e., the expected equilibrium warming for doubled CO₂ concentrations. The probability of exceeding a certain warming threshold is then calculated assuming a certain PDF for the climate sensitivity. Apparently, the estimates of this probability depend on the choice of a particular PDF for the climate sensitivity, introducing a certain degree of uncertainty (see the example mentioned above).

Over the last few years several studies have tried to constrain the climate sensitivity by recent observations. Murphy et al. (2004), for instance, obtained a 5–95% probability range of 2.4–5.4°C for the climate sensitivity on the basis of 53 different versions of the HadAM3 atmospheric general circulation model (“AGCM”) coupled to a mixed layer ocean model by varying various model parameters. In their study, the PDF is constrained by the choice of model parameters that are varied and their uncertainty ranges, specified on the basis of expert advice. The results from the ensemble are weighted according to their associated likelihood, given a range of present-day climate observations. Piani et al. (2005) extended this experiment to a multi-thousand member ensemble of simulations from the “climateprediction.net” project. In their study, however, the search for constraints on the response to increasing greenhouse gas levels is conducted with a systematic statistical methodology to identify correlations between the observables and the quantities to be predicted, i.e., the climate sensitivity and the climate feedback parameter. The authors came up with a best estimate of the climate sensitivity of 3.3°C and a 5–95% probability range of 2.2–6.8°C, when an internally consistent representation of the origins of model-data uncertainty is used. While the study by Piani et al. (2005) focused on linear predictors, the linearity condition was relaxed in the study by Knutti et al. (2006), using a neural network approach to establish a relation between climate sensitivity and the amplitude of the seasonal cycle in regional temperature. Most models with high sensitivities were found to overestimate the seasonal cycle compared to observations. Further, the climate sensitivity is very unlikely (5% probability) either below 1.5–2.0°C or above 5.0–6.5°C, with the best agreement found for sensitivities between 3.0 and 3.5°C. By this, the range is narrower than most probabilistic estimates derived from observed twentieth century warming.

Alternatively, one could estimate the allowable greenhouse gas concentrations for keeping the future warming below 2°C by directly using a comprehensive climate

model instead of estimates of the climate sensitivity of such models. That is, one prescribes the concentrations of the well-mixed greenhouse gases and of other forcing agents in such a way that the global warming does not exceed this threshold. The disadvantage of this method is that the magnitudes of the allowable greenhouse gas concentrations depend on the characteristics of the climate model, i.e., its climate sensitivity. In addition, the radiative transfer parameterizations in many coupled climate models are limited, either because they neglect particular absorbers, i.e., the near-infrared effects of CH₄ and N₂O, or because the methods for modelling the radiative processes themselves are limited (Collins et al. 2006). These shortcomings possibly render the estimates of the allowable greenhouse gas concentrations. The advantage, on the other hand, is that the effect of peaking time evolutions of greenhouse gas concentrations can be considered, such as those associated with a temporary overshooting as proposed by Meinshausen (2006), instead of constant greenhouse gas concentrations. Furthermore, the impact of the aerosol load can be considered, depending on the degree to which the various effects of aerosols are included in the climate model.

But a comprehensive climate model is the only means to assess the climatic changes associated with such a stabilization scenario in further detail. This is, however, necessary in order to evaluate how strongly the EU-target affects various aspects of climate and how big an improvement this means relative to higher emission scenarios, such as the SRES A1, A2, B1 and B2 families of scenarios proposed by the IPCC (Nakićenović et al. 2000). Each of these families represents different demographic, social, economic, technological and environmental developments but none of them includes additional climate initiatives, meaning that none of them explicitly assumes the implementation of the UNFCCC or the emission targets of the Kyoto Protocol. Hence, none of these scenarios considers mitigation initiatives.

Hansen and Sato (2004) proposed two additional scenarios for the well-mixed greenhouse gases, the so-called “2°C” and the so-called “Alternative” scenario, aiming at a future global warming of about 2 and 1°C, respectively, with respect to the year 2000. The 2°C scenario ends at an atmospheric CO₂ concentration of 560 ppm in 2100, while the Alternative scenario ends at a lower CO₂ concentration of 475 ppm. As for the Alternative scenario, this is achieved by a relatively weak (as compared to the SRES scenarios; Nakićenović et al. 2000) increase in the atmospheric CO₂ concentration until 2100. The atmospheric concentrations of the other well-mixed greenhouse gases follow different paths. The N₂O concentration, for instance, increases similarly to the SRES A1B scenario until 2100, while the CFC-11 and CFC-12 concentrations

are kept constant at the levels for 2000. The CH₄ concentration, on the other hand, peaks in 2000 and decreases markedly until 2050 and weakly until 2100. In Hansen et al. (2007) the GISS modelE coupled climate model was forced with these two scenarios, together with three of the SRES scenarios. It was found that the Alternative scenario keeps the future global warming below 1°C above the level in 2000 if the climate sensitivity is about 3°C or less for doubled CO₂. Furthermore, the Alternative scenario keeps the mean regional seasonal warming within two times the standard deviation of the observed variability for the twentieth century, while the other scenarios yield regional changes of 5–10 times the standard deviation. The authors also found evidence that an added global warming of more than 1°C above the level for 2000 already has effects that may be highly disruptive. Meehl et al. (2005) performed simulations with two different coupled climate models, stabilizing the CO₂ concentrations at the level for 2000. With respect to the pre-industrial period, the model with the weaker climate sensitivity (PCM) gives a global warming of 1.2°C by the end of the twenty-first century and the model with the higher climate sensitivity (CCSM3) a global warming of 1.6°C. When forced with the SRES B1 scenario, the PCM model gives a global warming just around 2°C by the end of the twenty-first century, while the CCSM3 model gives a global warming of 2.4°C.

In this study a somewhat different approach is chosen. Instead of prescribing a certain scenario for the well-mixed greenhouse gases similar to the Alternative scenario proposed by Hansen and Sato (2004), the greenhouse gas concentrations are chosen so that the future global warming simulated by the ECHAM5/MPI-OM coupled climate model does not exceed 2°C with respect to pre-industrial times. In addition, the anthropogenic sulphate aerosol load and stratospheric ozone concentrations for obtaining such a stabilization scenario are considered. Most importantly, the climatic changes associated with this so-called “2°C-stabilization” scenario are assessed in further detail, considering a variety of meteorological and oceanic variables. By this, the results presented here, supplement the fourth assessment report by the IPCC (“AR4”) in that such a scenario can only be achieved by mitigation initiatives, which have not been considered in any of the SRES scenarios. The climatic changes associated with the stabilization scenario are assessed in further detail, considering a variety of meteorological and oceanic variables, and compared to the respective changes associated with the SRES A1B scenario (Nakićenović et al. 2000). The A1B scenario leads to a markedly stronger warming with respect to pre-industrial times than the 2°C for the stabilization scenario (Meehl et al. 2007). The A1B scenario is the one of the three emission scenarios considered in AR4, for which alternative developments of energy technologies are

“balanced” with those based on fossil fuels. Also, the impact of the anthropogenic sulphate aerosol load and stratospheric ozone levels on the simulated climatic changes is investigated by comparing two simulations with different magnitudes of the anthropogenic sulphate aerosol load and of the stratospheric ozone concentrations.

The paper is organized as follows: the coupled climate model and the different model experiments performed in this study are introduced in Sect. 2. In the following sections the simulated changes in various meteorological and oceanic variables are discussed, i.e., the global mean changes in Sect. 3, the zonal mean changes in Sect. 4 and the local changes in Sect. 5, respectively. A summary and the conclusions are given in Sect. 6.

2 Model and experimental design

2.1 Model description

The model used is the Hamburg coupled atmosphere–ocean model, combining the ECHAM5 atmospheric general circulation model (Roeckner et al. 2003, 2006) and the MPI-OM ocean/sea-ice model (Marsland et al. 2003). ECHAM5 uses the spectral transform method for vorticity, divergence, temperature and the logarithm of surface pressure at T63 horizontal resolution with 31 levels in a hybrid sigma/pressure coordinate system in the vertical with the top level at 10 hPa. It uses state-of-the-art parameterizations for shortwave and longwave radiation, stratiform clouds, boundary layer and land-surface processes, and gravity wave drag. The direct aerosol effect is calculated by transforming the prescribed sulphate mass into number concentrations assuming a log-normal size distribution and considering the dependence of particle size on ambient relative humidity (Hess et al. 1998). The first indirect effect (Twomey 1977) is included via empirical relationships between sulphate mass and the cloud droplet number concentration (Boucher and Lohmann 1995). Neither the second indirect effect of sulphate aerosols nor the effects of black and organic carbon are considered in the version of the AGCM used here. Roeckner et al. (2006) added a detailed representation of tropospheric aerosols to the ECHAM5/MPI-OM (together with a model of the marine biogeochemistry) in order to investigate the impact of carbonaceous aerosols on regional climate. They found a negligible impact of projected changes in carbonaceous aerosols on the global mean temperature but significant changes at low latitudes. The detailed description of the tropospheric aerosols, however, has not been used in the simulations presented here, since it is heavily demanding on computer resources. In the simulations time-varying concentrations of the well-mixed greenhouse gases have

been prescribed, according to observational estimates until the year 2000 and according to the SRES A1B scenario in the following years. The time-varying concentrations of ozone and sulphate aerosols have been specified according to pre-calculated values for prescribed emissions of precursor components (Kiehl et al. 1999, O. Boucher, personal communication, 2004).

MPI-OM employs the primitive equations for a hydrostatic Boussinesq fluid with a free surface at a resolution of 1.5° and a vertical discretization at 40 *z*-levels. The poles of the curvilinear grid are shifted to land areas over Greenland and Antarctica. Parameterized processes include along-isopycnal diffusion, horizontal tracer mixing by advection with unresolved eddies, vertical eddy mixing, near-surface wind stirring, convective overturning, and slope convection. Concentration (i.e., the fraction of an ocean grid cell covered by sea-ice) and thickness of sea-ice are simulated by a dynamic and thermodynamic sea-ice model. In the coupled model (Jungclaus et al. 2006), the ocean passes to the atmosphere the sea-surface temperature, sea-ice concentration and thickness, snow depth on ice, and ocean surface velocities. Using these boundary values, the AGCM accumulates the forcing fluxes (wind stress, heat, freshwater including river runoff and glacier calving, and 10 m wind speed) during the coupling time step of one day and passes the daily mean fluxes to the ocean model. All fluxes are calculated separately for ice-covered and open water partitions of the grid cells.

The performance of the ECHAM5/MPI-OM coupled climate model was investigated in Jungclaus et al. (2006), focussing on some key features of the ocean, i.e., sea surface temperatures (“SSTs”), the large-scale circulation, meridional heat and freshwater transports and sea-ice, and the tropical variability. They found that the simulation of the SSTs and the sea-ice conditions is both stable and realistic. Global-scale heat and freshwater transports are in broad agreement with observations, and the improved compatibility of the ocean and atmospheric heat budget allows for simulating a stable climate without flux

adjustment. The North Atlantic overturning circulation and the associated heat and freshwater transports are stable. There is, however, insufficient Antarctic Bottom Water (“AABW”) formation, leading to a significant reduction of the AABW overturning cell. As for the tropics, the cold bias of the SSTs in the tropical Pacific in a previous version of the climate model has been reduced by more than 1°C and the simulation of the tropical variability is improved. The strength of the variability is reduced as well as the extension of the variability into the western tropical Pacific Ocean. The period of the El Niño events is more realistically simulated, with a dominant period of about 4 years.

2.2 Model experiments

The ECHAM5/MPI-OM coupled model has been used for several simulations with varying concentrations of well-mixed greenhouse gases, i.e., CO₂, CH₄, N₂O, CFC-11, and CFC-12, of both tropospheric and stratospheric ozone, and of sulphate aerosols prescribed. In one simulation over the period 1861–2200, the concentrations of these substances have been prescribed according to observations until the year 2000 and according to the SRES A1B scenario (Nakićenović et al. 2000) for the period 2001–2100. As for ozone, however, only the changes in the stratospheric ozone are prescribed according to the A1B scenario but annually cyclic distributions based on observations are used for the tropospheric ozone (Meehl et al. 2007). In the period 2101–2200 all concentrations have been kept constant at the level of the year 2100. This simulation (referred to as “A1B” in the following; see Table 1) shows a warming of 3.47°C with respect to pre-industrial times in the period 2071–2100 (also referred to as “the end of the twenty-first century” in the following) and of 4.71°C in the period 2171–2200 (also referred to as “the end of the twenty-second century” in the following) due to the prescribed anthropogenic changes in the greenhouse gas concentrations (see Table 2).

Table 1 List of experiments with both constant (“Const”) and time-varying (“Var”) prescription of the various forcing agents

Experiment	Period	CO ₂ , CH ₄ , N ₂ O, CFC-11, and CFC-12	O ₃ and SO ₄
A1B	1861–2200	Var observations (1861–2000)	Var observations (1861–2000)
		Var A1B scenario (2001–2100)	Var A1B scenario (2001–2100)
		Const A1B (2100; 2101–2200)	Const A1B (2100; 2101–2200)
2C20	2020–2200	Const A1B (2020)	Var A1B scenario ^a (2020–2036) Const A1B (2100; 2037–2200)
2C25	2025–2100	Const A1B (2025)	Var A1B scenario ^a (2025–2040) Const A1B (2100; 2041–2100)
2C30	2030–2100	Const A1B (2030)	Var A1B scenario ^a (2030–2044) Const A1B (2100; 2045–2100)
2C30A	2030–2100	Const A1B (2030)	Const A1B (2030)

^a These revised scenarios for O₃ and SO₄ approach the levels for the year 2100 (according to the A1B scenario) five times as fast as for the original A1B scenario (see text for details)

In the experiments presented here, the concentrations of the well-mixed greenhouse gases as well as the sulphate aerosol load and the stratospheric ozone concentration have been prescribed in such a way that the global warming with respect to pre-industrial times, i.e., the period 1861–1890, does not exceed 2°C by the end of the twenty-first century, without actually exceeding this threshold before that point in time. It could, however, happen that the warming exceeds the threshold at a later stage since the coupled model may not have reached its equilibrium at the end of the twenty-first century and the global mean temperature continues to increase. This additional increase in the global mean temperature, which is due to the inertia of the climate system, in particular the inertia of the ocean, is often referred to as “unrealized warming”. Since the main goal of this study is to assess the climatic changes associated with a 2°C-stabilization scenario close to equilibrium, the levels of the various forcing agents have been kept constant at a certain point in time. That is, that the changes in the emission rates of the forcing agents are as high as the rates at which these constituents are removed from the atmosphere.

A1B shows a warming of 0.97°C for the period 2001–2030 and an unrealized warming of 1.24°C between the periods 2071–2100 and 2171–2200, i.e., over the first 100 years of simulation with constant levels of the various forcing agents. Assuming a smaller unrealized warming at an earlier point in time, one can expect a warming of 2°C by the end of the twenty-first century when starting the simulation in 2030 with starting conditions from A1B, keeping the greenhouse gas concentrations at the level of 2030 and stratospheric ozone and sulphate at the level of 2100. In this simulation (“2C30”), the concentrations of stratospheric ozone and sulphate aerosols are changed to the levels for 2100 according to the A1B scenario over a period of 15 years, i.e., five times as fast as in A1B, and kept constant through the rest of the simulation. That is, in 2C30 the concentrations of ozone and sulphate aerosols for 2031, 2032, 2033, ..., 2043 and 2044 correspond to the

respective concentrations for 2035, 2040, 2045, ..., 2095 and 2100 in A1B. But since this simulation exceeds the 2°C threshold by the end of the twenty-first century by 0.13°C (see Table 2), another simulation is started in 2025 with a weaker warming of 0.84°C during the period 1996–2025. But also this simulation (“2C25”) exceeds the 2°C threshold by 0.04°C, making a third simulation (“2C20”) necessary, starting in 2020 with a warming of 0.73°C for the period 1991–2020. The atmospheric concentrations of the well-mixed greenhouse gases for the year 2020 are 418 ppm (CO₂), 2026 ppb (CH₄), 331 ppb (N₂O), 786 ppt (CFC-11) and 486 ppt (CFC-12), respectively. This simulation gives a warming of 1.92°C by the end of the twenty-first century (see Table 2), so that the aforementioned greenhouse gas concentrations define the so-called 2°C stabilization scenario. In this simulation, the stratospheric ozone concentrations and the sulphate aerosol loads for 2021, 2022, 2023, 2024, 2025, ..., 2035 and 2036 correspond to those for 2025, 2020, 2035, 2040, 2045, ..., 2095 and 2100 in A1B. Hence, the anthropogenic sulphate aerosol load decreases from the level for 2020 to 0.23 TgS in the global annual mean for 2036, staying at this level throughout the rest of the simulation.

In order to evaluate the dependence on the particular choice of the anthropogenic sulphate aerosol load and of the ozone levels, an additional simulation (“2C30A”) was performed that just as 2C30 started in 2030 with the greenhouse gas concentrations for 2030 but also with the stratospheric ozone concentrations and sulphate aerosol load at the level of 2030 according to the A1B scenario. This scenario gives global anthropogenic sulphur dioxide (“SO₂”) emissions of 92 TgS/year in 2030 and of 28 TgS/year in 2100 (Nakićenović et al. 2000). According to a simulation of the global sulphur cycle implemented in a AGCM, these emissions lead to annual mean global anthropogenic sulphate aerosol burdens of 0.69 TgS in 2030 and 0.23 TgS in 2100, respectively (Boucher et al. 2002; Pham et al. 2005). Three-dimensional sulphate aerosol distributions originating from this simulation have actually been prescribed to the ECHAM5/MPI-OM on a monthly basis. The stratospheric ozone concentrations, on the other hand, are lower in 2030 than for 2100. The largest annual mean differences in the ozone concentrations occur in the upper stratosphere at high latitudes, i.e., the concentrations in the Southern (Northern) Hemisphere are about 300 ppb (140 ppb) lower in 2030 than in 2100. As a consequence, 2C30A is forced by both a higher sulphate aerosol load and lower stratospheric ozone concentrations as compared to 2C30. The higher sulphate aerosol load and lower stratospheric ozone concentrations in 2C30A lead to a weaker warming of 1.60°C by the end of the twenty-first century compared to 2.13°C for 2C30 (see Table 2). This is consistent with the estimated negative radiative forcing of

Table 2 Change in global annual mean near-surface temperature for two periods with respect to the period 1861–1890

Experiment	Period 2071–2100	Period 2171–2200
A1B	3.47	4.71
2C20	1.92	2.02
2C20M	1.88	2.06
2C20D	1.94	
2C25	2.04	
2C30	2.13	
2C30A	1.60	

Units are °C

the increased sulphate aerosols load due to the direct and the first indirect effect of about 0.7 W/m² through the period 1750–2005 (Forster et al. 2007).

Ideally, the experiment with the higher sulphate aerosol load should have been started in the year 2020, i.e., in the same year as the 2°C stabilization scenario, instead of 2030. 2C30A, however, was the first experiment that has been performed and, hence, already available, so that this would have meant to run an additional simulation. But since the comparison between 2C30A and 2C30 presumably leads to the same conclusions as the comparison between such an additional simulation, which would be referred to as “2C20A”, and 2C20, the results from the comparison between 2C30A and 2C30 are presented in the further course of this study.

3 Global mean changes

In this section, time series of the annual mean changes in the global mean temperature and daily precipitation, of the annual mean radiative forcing as well as of the seasonal mean changes in the sea-ice extent and sea-ice volume in the Arctic and the Antarctic region, respectively, are considered. More precisely, these time series represent changes in the 30-year running averages or 30-year running averages, respectively, of the particular variables with respect to the pre-industrial period 1861–1890.

3.1 Near-surface temperature

A1B shows a continuous warming relative to pre-industrial times (with a value of 14.03°C for the period 1861–1890; see Table 3) throughout almost the entire period 1861–2200, with 3.47°C by the end of the twenty-first century and 4.71°C by the end of the twenty-second century (Fig. 1a). This is a warming of 3.03 and 4.27°C, respectively, relative to the period 1971–2000. By this, A1B gives

Table 3 Averages over the period 1861–1890 “reference values” for the variables considered in Figs. 1, 2, 3 and 4

Variable	Annual	
	January–March	July–September
Temperature in 2 m	14.03°C	
Precipitation	2.91 mm/day	
NH sea-ice cover	13,576,000 km ²	7,144,000 km ²
NH sea-ice volume	34,400 km ³	23,600 km ³
SH sea-ice cover	3,146,000 km ²	13,220,000 km ²

NH Northern Hemisphere, SH Southern Hemisphere

a somewhat higher value than the average warming of 2.80 and 3.50°C relative to the period 1980–1999 for the end of the twenty-first and the end of the twenty-second century, respectively, for the SRES A1B scenario according to AR4 (Meehl et al. 2007). As for the end of the twenty-first century, A1B is well inside the standard deviation of the 21 different model simulations considered, but for the end of the twenty-second century the difference between A1B and the average of the 17 simulations considered is close to the standard deviation. The somewhat stronger warming simulated by ECHAM5/MPI-OM is consistent with the estimates of the radiative forcing of a doubled CO₂ concentration for this climate model. According to Forster and Taylor (2006), the net forcing for ECHAM5 is 4.01 W/m² as compared to the average value of 3.75 W/m² with a standard deviation of 0.23 W/m², considering nine different coupled climate models. Consistent with this, the diagnosed climate feedback term from the doubled CO₂ simulations is 1.24 W/m² per Kelvin for ECHAM5 as

Near-surface temperature

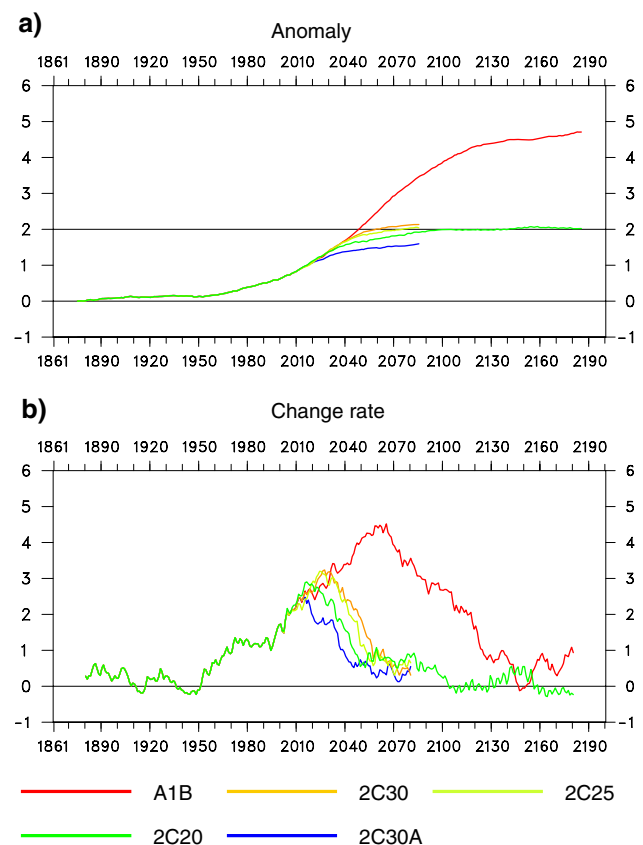


Fig. 1 Changes in the 30-year averages of global annual mean near-surface temperature with respect to the period 1861–1890 (a) and 10-year running means of the year-to-year differences of these 30-year averages (b) for the different experiments. Units are °C (a) and °C/century (b). The years indicate the centres of the 30-year periods

compared to $1.20 \pm 0.30 \text{ W/m}^2$ per Kelvin for the average of these models.

In A1B, the strongest warming rate of more than $4.5^\circ\text{C}/\text{century}$ occurs around 2060 (Fig. 1b), in response to both a strong increase in all greenhouse gas concentrations except CH_4 and a marked decrease in the anthropogenic SO_2 emissions (Nakićenović et al. 2000), leading to a reduction in the anthropogenic sulphate aerosol load. After the concentrations of the well-mixed greenhouse gases and of the sulphate aerosols are kept constant at the level of 2100, the warming continues throughout the rest of the simulation, particularly during the first 30 years after the stabilization of the forcing agents with more than $1^\circ\text{C}/\text{century}$.

For the other experiments, the strongest warming rates reach only between 2.5 and $3.5^\circ\text{C}/\text{century}$ shortly after the greenhouse gas concentrations are kept constant (Fig. 1b). A minor part of the warming is due to the decreasing anthropogenic sulphate aerosol load and the increasing stratospheric ozone levels over the first 15 (2C30), 16 (2C25) and 17 years (2C20) of the simulations. After reaching their respective maxima, the warming rates decrease over the following 30 years and stay at about $1^\circ\text{C}/\text{century}$ thereafter. For 2C20, the warming rate eventually (around the year 2100) is close to $0^\circ\text{C}/\text{century}$, indicating that this simulation has almost reached its equilibrium. Starting from 0.73°C in 2020, 2C20 stays below a warming of 2°C until the mid of the twenty-second century, reaching a maximum warming of 2.07°C a few decades later (Fig. 1a). The global warming of 2°C in 2C20 is well below the warming associated with the various SRES scenarios presented in AR4 (Meehl et al. 2007). The B1 scenario with the weakest increases in the concentrations of the well-mixed greenhouse gases, for instance, leads to a global warming of $2.5 \pm 0.4^\circ\text{C}$ with respect to pre-industrial times at the end of the twenty-first century. Hence, the corresponding simulation with PCM (Meehl et al. 2005), which is also included in AR4, is just outside the standard deviation with a global warming of about 2.0°C . Similar to 2C20, also in Hansen et al. (2007) the global warming associated with the Alternative scenario at the end of the twenty-first century is 0.5°C weaker than the warming for the B1 scenario.

The higher sulphate aerosol load and lower stratospheric ozone levels in 2C30A lead to a relatively weak warming in this experiment with 1.60°C by the end of the twenty-first century (Fig. 1a), which is 0.53°C less than for 2C30. Consistent with this, also the warming rate is generally weaker in 2C30A than in 2C30 (Fig. 1b). The marked cooling effect of the higher anthropogenic sulphate aerosol load is related to both the direct and the first indirect effect of these aerosols (Brasseur and Roeckner 2005). Based on an earlier study by Roeckner et al. (1999), Lohmann and Feichter (2005) diagnosed the effective radiative forcing

using the preceding version of the ECHAM5 AGCM, ECHAM4, as -0.28 W/m^2 for the direct and as -0.90 W/m^2 for the first indirect effect of sulphate aerosols. This estimate of the first indirect effect is similar to another estimate by Rotstajn and Penner (2001), while the estimate of the direct effect is only about half as strong as the estimate by Rotstajn and Penner (2001). The second indirect or lifetime effect of sulphate aerosols, which is not considered in the ECHAM5 AGCM, has about the same magnitude as the first indirect effect, i.e., -1.03 W/m^2 as compared to -1.12 W/m^2 (Rotstajn and Penner 2001). As a consequence, the relatively weak future warming in 2C30A would be even more reduced, if also the second indirect effect of the sulphate aerosols was considered in the version of the ECHAM5/MPI-OM coupled climate model used here. When totally removing the anthropogenic sulphate aerosol load from the atmosphere, Brasseur and Roeckner (2005) found an additional warming of 0.80°C for the year 2000 due to the improved air quality. This is somewhat more than the difference of 0.53°C between 2C30 and 2C30A, reflecting the fact that in Brasseur and Roeckner (2005) the anthropogenic SO_2 emissions were reduced more (by about $70 \text{ TgS}/\text{year}$ for the global mean) than in the experiments presented here. The consideration of carbonaceous aerosols in the coupled model used here would possibly also affect the magnitude of the future warming. While the direct radiative forcing of particulate organic matter is generally, that is in most models considering carbonaceous aerosols, negative, the forcing associated with black carbon is generally positive (Schulz et al. 2006). Hence, the relatively weak warming in 2C30A would be enhanced, if the radiative effect of black carbon was considered under the assumption of a higher black carbon aerosol load in 2030 than in 2100 similar to the sulphate aerosols.

The idealized case of keeping the concentrations of the well-mixed greenhouse gases constant at a certain point in time, which is chosen in this study, requires that the anthropogenic emission rates of these forcing agents are balanced by the rates at which these constituents are removed from the atmosphere. Given the different residence times of the various greenhouse gases, i.e., 12 ± 3 years for CH_4 , 120 years for N_2O , 45 years for CFC-11, 100 years for CFC-12 and the potentially very long residence time for CO_2 (e.g., Solomon et al. 2007), a more realistic case would be continuing slight increases in the concentrations of CO_2 and N_2O up until 2050 or 2100 and a peaking concentration of CH_4 after about a decade and a subsequent reduction. The so-called Alternative scenario proposed by Hansen and Sato (2004) is actually based on such kinds of emissions paths. Meinshausen (2006) proposes such emission pathways in an emission scenario stabilizing the greenhouse gas concentrations at

475 ppm equivalent CO₂, at which the probability of reaching the EU-target is found at “medium likelihood” or “unlikely”. Stabilization at a considerably lower equivalent CO₂ level such as 400 ppm would, however, require marked reductions in the atmospheric CO₂ concentrations in the second half of the twenty-first century after an overshooting in the first part of the century.

In order to investigate whether the magnitude of the global warming and, hence, the greenhouse gas concentrations for keeping the global warming below 2°C depends on the emission paths, another simulation, with peaking greenhouse gas concentrations in 2035 has been performed. In this simulation, referred to as “2C20D”, the atmospheric concentrations of the well-mixed greenhouse gases continue to increase until 2035 according to the SRES A1B scenario, before they are reduced to the levels for 2020 (reaching them in 2050), while the stratospheric ozone concentrations and the anthropogenic sulphate aerosol load are prescribed as in 2C20. That is, the allowable greenhouse gas concentrations (according to 2C20) are reached 30 years later than in 2C20 and are exceeded in the period 2020–2050 for all forcing agents but CFC-12. The particular forcing agents reach their maxima of 465 ppm (CO₂), 2,270 ppb (CH₄), 341 ppb (N₂O) and 791 ppt (CFC-11) and the minimum of 421 ppt (CHC-12), respectively, in 2035. Due to the stronger radiative forcing of the greenhouse gases, 2C20D shows a stronger warming of the global mean temperatures than in 2C20 through the entire twenty-first century (Fig. 2a) with 1.94°C at the end of the twenty-first century as compared to 1.92°C for 2C20 (see Table 2). That is, despite the temporary overshooting of the greenhouse gas concentrations the target of keeping the global warming below 2°C can be achieved if the concentrations are subsequently reduced. The temporal evolution of the change rate indicates the very weak increase of the global mean temperature once the greenhouse gas concentrations start to decrease in 2035 (Fig. 2b). It also shows that 2C20D is much closer to equilibrium than 2C20 by the end of the twenty-first century.

Another interesting issue is whether the estimates of the concentrations of the well-mixed greenhouse gas for keeping the global warming below 2°C by the end of the twenty-first century depend on the climatic state of the coupled climate model. Therefore, another simulation similar to 2C20 has been performed, referred to as “2C20M”. In this simulation, the atmospheric concentrations of the well-mixed greenhouse gases and stratospheric ozone as well as the anthropogenic sulphate aerosol load are prescribed as in 2C20 but the simulation was started from a different climatic state originating from a simulation corresponding to A1B performed at the Max-Planck-Institute for Meteorology (“MPI”) in Hamburg. 2C20M is

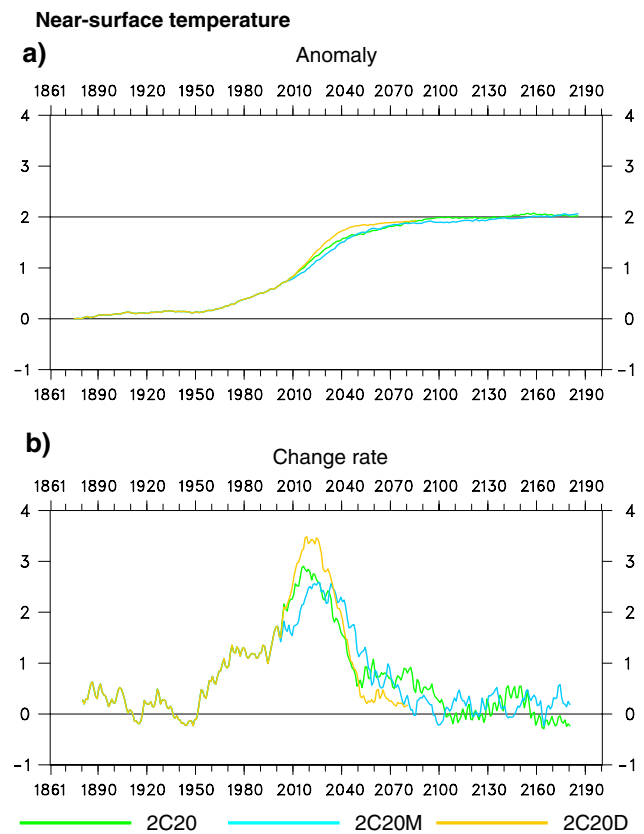


Fig. 2 As Fig. 1, but for 2C20, a corresponding simulation starting from a different climate state (“2C20M”) and a corresponding simulation with a delayed stabilization of the greenhouse gas concentrations (“2C20D”)

colder than 2C20 for about 50 years, reaching the same change in temperature at about 2060 (Fig. 2a). One reason for this is the colder climate state of the simulation provided by MPI, the other is the relatively weak warming during the first 10 years of 2C20M (Fig. 2b). The warming of more than 0.5°C/century continues about 10 years longer in 2C20M, leading to the same temperature change at about 2060. Also after about 2060, variations at decadal time scales give rise to small differences between 2C20M and 2C20, resulting in a warming of 1.88°C by the end of the twenty-first century in 2C20M as compared to 1.92°C in 2C20 (see Table 2). Furthermore, 2C20M exceeds the threshold of 2°C about 20 years later than 2C20.

3.2 Radiative forcing

In order to better describe the effects of the different concentrations of the well-mixed greenhouse gases and of the different sulphate aerosol loads more directly, the radiative forcing has been computed for the different simulations. This has been done on the basis of the methodology described in Forster and Taylor (2006), giving

rather accurate estimates of the radiative forcing despite its simplified linear approach. The estimates based on this method were diagnosed to agree with the conventional estimates of the radiative forcing within 10% for both the longwave and the shortwave component.

The approach relies on a simple globally averaged linear forcing feedback model. Adopting the terminology from Gregory et al. (2004a, b), the net flux imbalance of the climate system (N) can be described as

$$N = Q - Y \cdot \Delta T_s, \quad (1)$$

in relation with the radiative forcing (Q), the globally averaged surface temperature change (ΔT_s) and the climate feedback factor (Y). The latter is the inverse of the climate sensitivity. This equation is approximate as it only considers climate feedbacks that are proportional to global mean temperature changes, i.e., the parts of the energy budget from clouds, water vapour, surface albedo and lapse rate change. These temperature changes are mainly governed by the ocean mixed layer relaxation time. Therefore, this equation may not accurately reflect the impact of more slowly responding aspects of climate, such as ice sheets or the carbon cycle. These aspects of climate, however, are not considered in the ECHAM5/MPI-OM coupled climate model, which is used here.

According to Forster and Taylor (2006), ECHAM5/MPI-OM gives estimates of the climate feedback factor of $2.04 \pm 0.18 \text{ W/m}^2$ per Kelvin for the longwave radiative fluxes, of $-0.92 \pm 0.18 \text{ W/m}^2$ per Kelvin for the shortwave radiative fluxes and of $1.12 \pm 0.17 \text{ W/m}^2$ per Kelvin for the total radiative fluxes. As for the longwave and the total radiative fluxes, this is somewhat weaker than the average of the 20 coupled climate models considered in that study (2.31 and 1.42 W/m^2 per Kelvin), respectively, for the shortwave radiative fluxes this is slightly stronger than the average (-0.89 W/m^2 per Kelvin).

According to this analysis, all experiments give a positive longwave radiative forcing (Fig. 3b), largely in association with the prescribed increases in the concentrations of the well-mixed greenhouse gases (Fig. 3b). By the end of the twenty-first century, 2C20 gives a longwave radiative forcing of 3.11 W/m^2 compared to 5.86 W/m^2 for A1B (see Table 4), reflecting the different magnitudes of the greenhouse gas concentrations. Correspondingly, 2C25, 2C30 and 2C30A give slightly higher estimates of the longwave radiative forcing than 2C20. In 2C20, the longwave radiative forcing is only very slightly enhanced by the end of the twenty-second century, while in A1B the longwave radiative forcing goes up to 6.85 W/m^2 , since this simulation has not reached its equilibrium yet. As for the shortwave radiative fluxes, on the other hand, all experiments give a negative radiative forcing (Fig. 3a), largely in association with the anthropogenic sulphate

Radiative forcing

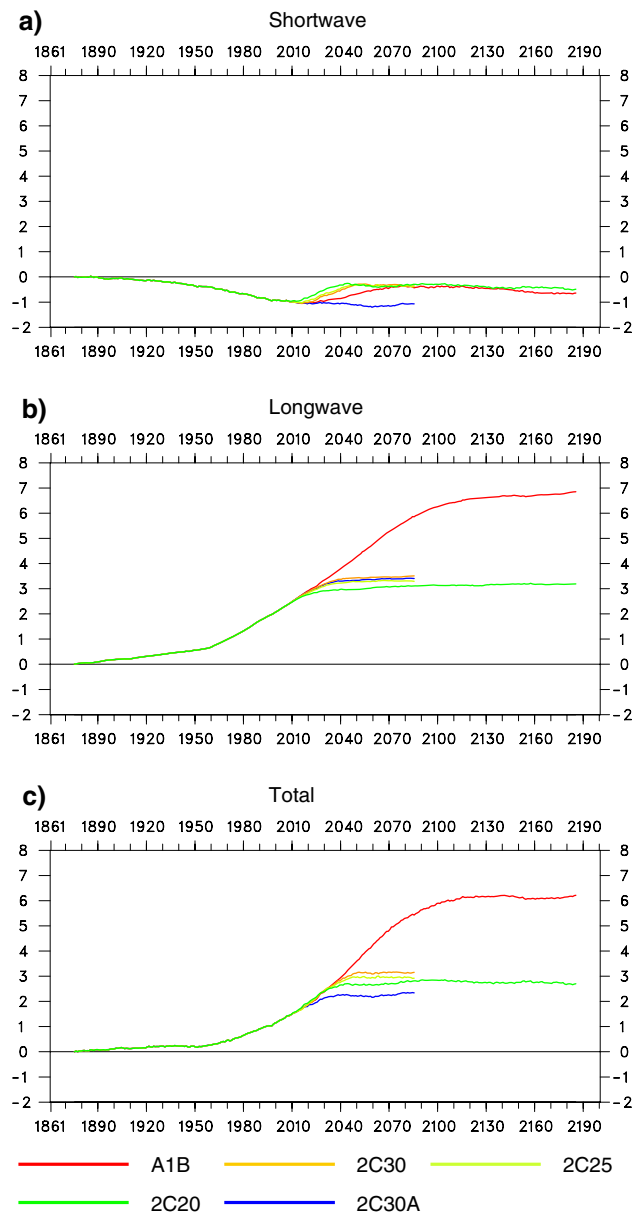


Fig. 3 Thirty-year averages of global annual mean radiative forcing with respect to the period 1861–1890 for **a** the shortwave, **b** the longwave and **c** the total radiative fluxes for the different experiments. Units are W/m^2

aerosol burden. As a consequence of the higher sulphate aerosol burden, 2C30A gives a shortwave radiative forcing of 1.07 W/m^2 by the end of the twenty-first century, while all other experiments give a considerably weaker shortwave radiative forcing between -0.29 W/m^2 (2C20) and -0.43 W/m^2 (A1B; see Table 4). The estimate for A1B is somewhat stronger than for the three other simulations because this simulation reaches the same anthropogenic sulphate aerosol burden as in the other three simulations not before 2100. In contrast to the longwave radiative

Table 4 Global annual mean radiative forcing, distinguishing between the shortwave (“SW”), the longwave (“LW”) and the total (SW + LW) radiative fluxes, for two periods with respect to the period 1861–1890

Experiment	Period 2071–2100			Period 2171–2200		
	SW	LW	SW + LW	SW	LW	SW + LW
A1B	−0.43	5.86	5.43	−0.64	6.85	6.21
2C20	−0.29	3.11	2.82	−0.49	3.19	2.70
2C25	−0.38	3.29	2.92			
2C30	−0.36	3.51	3.15			
2C30A	−1.07	3.41	2.34			

Units are W/m^2

forcing, 2C20 and A1B give about the same shortwave radiative forcing by the end of the twenty-second century (−0.49 and −0.64 W/m^2 , respectively; see Table 4). Since the longwave radiative forcing exceeds the shortwave radiative forcing in all simulations at all times, the total radiative forcing is positive throughout the entire time period for all experiments and clearly reflects the differences between the various simulations (Fig. 3c). That is, A1B and 2C30A with the strongest (weakest) future global warming (see Fig. 1a) give the strongest (weakest) radiative forcing, while for the three other simulations, 2C20, 2C25 and 2C30, the relative strength of the radiative forcing follows the relative strength of the future global warming in these simulations.

3.3 Precipitation

Also the simulated changes in the global annual mean daily precipitation show a continuous increase throughout almost the entire period (Fig. 4a). The increases reach 0.18 mm/day for A1B and 0.10 mm/day for 2C20 by the end of the twenty-first as well as 0.26 mm/day (A1B) and 0.12 mm/day (2C20) by the end of the twenty-second century. The latter numbers correspond to an increase of 8.9 and 4.1%, respectively, relative to pre-industrial times (2.91 mm/day; see Table 3). The two simulations starting at 2030 show increases of 0.07 mm/day (2C30A) and 0.12 mm/day (2C30), illustrating a 2% weaker increase in daily precipitation associated with the weaker warming as a consequence of the higher anthropogenic sulphate aerosol load. This is, again, consistent with the results by Brasseur and Roeckner (2005), who found a somewhat stronger increase of the globally averaged precipitation by 3% as a consequence of the removal of the anthropogenic sulphate aerosol load.

By this, the changes in the global mean daily precipitation in the various experiments follow by and large the corresponding changes in the near-surface temperature (see Fig. 1a), that is the stronger the global warming is, the

Precipitation

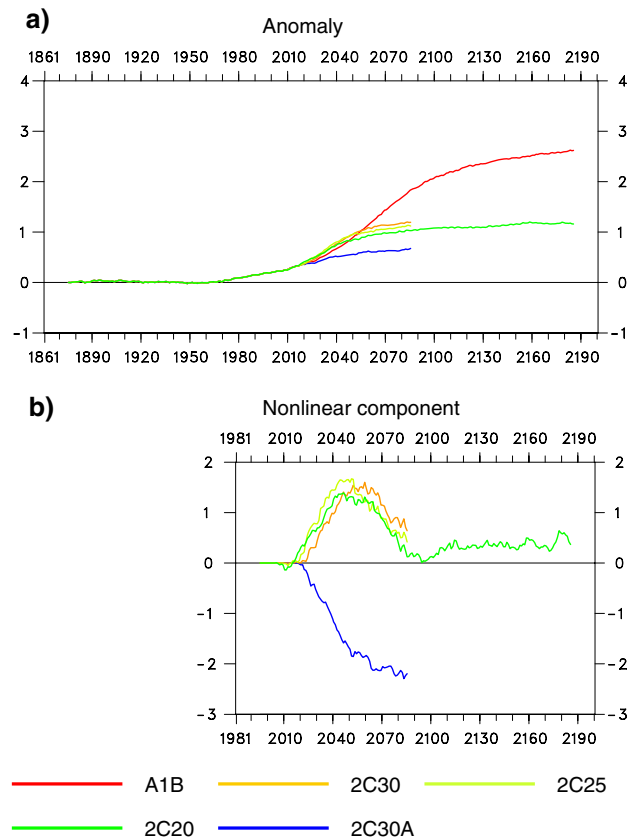


Fig. 4 Changes in the 30-year averages of global annual mean daily precipitation with respect to the period 1861–1890 (a) and the nonlinear components of these changes (b) for the different experiments. Units are 1/10 mm/day (a) and 1/100 mm/day (b)

stronger is the corresponding future change in global mean daily precipitation. However, the change in global mean precipitation is not a linear function of the change in global mean temperature as shown, for instance, in the supplementary materials of Chap. 10 in AR4 (Meehl et al. 2007). According to their findings, the strongest (weakest) changes in global mean precipitation scaled with the corresponding changes in global mean temperature, the so-called “hydrological sensitivity”, occur for the SRES B1 (A2) scenario with the weakest (strongest) global warming. Moreover, the hydrological sensitivity is found to be considerably higher for aerosol forcing than for greenhouse gas forcing (Feichter et al. 2004).

In order to assess the differences in the hydrological sensitivity for the various experiments in this study, the nonlinear component of the changes in global mean daily precipitation is analyzed. Following the approach originally proposed by Mitchell et al. (1999) and applied to both global (e.g., Mitchell 2003) and regional climate changes (e.g., Räisänen et al. 2004; Giorgi 2005), the linear component of the change in the quantity X such as the global

mean precipitation for a given scenario “x” and a reference scenario “ref” can be approximated by

$$\Delta X_x^{\text{lin}} = \frac{\Delta X_{\text{ref}}}{\Delta T_{\text{ref}}} \times \Delta T_x, \quad (2)$$

where ΔT is the change in the global mean temperature. Then the nonlinear component of the change in X follows as

$$\Delta X_x^{\text{nl}} = \Delta X_x - \Delta X_x^{\text{lin}}. \quad (3)$$

In order to analyze the nonlinear component of the changes related to the different magnitudes of the well-mixed greenhouse gas concentrations, A1B is used as the reference scenario for 2C20, 2C25 and 2C30. For 2C30A, on the other hand, 2C30 is used as the reference scenario. This allows for estimating the nonlinear component of the changes due to the higher anthropogenic sulphate aerosol load. In the further course of this study, the linear and nonlinear components have not only been computed for time series of the changes with respect to the pre-industrial period but also for the changes in the zonal means as well as for the local changes between the mean values for two periods presenting the present-day and the future climate for various meteorological variables.

As for global mean daily precipitation, the nonlinear component of the changes is positive for the three scenarios with the reduced greenhouse gas concentrations (2C20, 2C25 and 2C30) throughout the simulation (Fig. 4b). This indicates that in these experiments the weaker global warming leads to stronger (in a relative sense) increases in precipitation, consistent with the findings by Meehl et al. (2007). As for 2C20, the magnitude of the nonlinear component varies between 0.003 and 0.005 mm/day during the twenty-second century, the period when the greenhouse concentrations are kept constant at the respective levels in both 2C20 and A1B and the anthropogenic sulphate aerosol load is kept constant at the same level. In the beginning of 2C20, when the sulphate aerosol load is considerably smaller than in A1B, the nonlinear component of the change exceeds 0.10 mm/day for an extended period. Only towards the end of the twenty-first century, when the anthropogenic sulphate aerosol load approaches the same level as in A1B, the nonlinear component comes close to 0.005 mm/day. The maxima of the nonlinear component of the changes in 2C25 and 2C30 occur about 5 and 10 years later than for 2C20 with slightly higher values. These delays are due to the fact that the lowest anthropogenic aerosol load is reached 5 (2C25) and 10 years (2C30) later than in 2C20. The higher magnitudes of the maxima are related to differences in the sulphate aerosol load, since 2C25 and 2C30 start from weaker SO₂ emissions of 96 (2C25) and 92 TgS/year (2C30) and, hence, smaller anthropogenic sulphate aerosol loads than 2C20

(100 TgS/year). The higher greenhouse gas concentrations, giving negative nonlinear components of the change in 2C25 and 2C30, apparently have a weaker effect than the lower sulphate aerosol loads.

As for 2C30A, i.e., the scenario with the higher anthropogenic sulphate aerosol load, the nonlinear component of the changes in the global mean daily precipitation is negative, exceeding -0.02 mm/day at the end of the twenty-first century, when the difference in the aerosol load is largest. Also considering other types of aerosols, i.e., organic and black carbon as well as mineral dust and sea salt, Feichter et al. (2004) found that the global hydrological sensitivity to a warming of 1°C is almost three times higher for aerosol forcing than for greenhouse gas forcing. Hence, they found a decrease in global mean evaporation and precipitation by 2% per degree Celsius despite a global warming of 0.57°C when combining these two forcings.

3.4 Sea-ice conditions

For the sea-ice cover and sea-ice volume in the Arctic and the Antarctic region, seasonal means are considered because of the strong annual cycle, distinguishing between the periods January–March (“JFM”) and July–September (“JAS”). Only grid boxes with at least 15% of the area covered by sea-ice in a particular month are included, following a widely used practice in both observational and modelling studies (e.g., Johannessen et al. 2004).

In the Arctic region, A1B shows a considerable reduction of the sea-ice cover by the end of the twenty-first century, i.e., by 3,675,000 km² in JFM (Fig. 5a) and 5,464,000 km² in JAS (Fig. 5b) with respect to pre-industrial times. By the end of the twenty-second century the reduction has reached 5,618,000 km² in JFM and 6,722,000 km² in JAS, corresponding to a reduction by 41% in late winter but 94% in late summer (see Table 3). As a consequence, the magnitude of the annual cycle of the sea-ice cover is enhanced in the future warmer climate. The different magnitudes of the changes indicate that the sea-ice cover is most sensitive to global warming in summer, the period with the minimum extent. This is because the future warming leads to near-surface temperatures above freezing in large parts of the Arctic region in summer and, hence, to a strong decline of the sea-ice. By the end of the twenty-second century, the Arctic sea-ice in September has totally disappeared in some years. AR4 gives very similar reductions of the sea-ice cover associated with the SRES A1B scenario by the end of the twenty-first century, i.e., about 3,000,000 km² in JFM and about 5,000,000 km² in JAS with respect to the period 1980–2000 (Meehl et al. 2007). A1B shows also a strong decrease in the Arctic sea-ice volume, i.e., by 24,200 km³ (JFM) and 22,100 km³

Sea-ice conditions—Northern Hemisphere

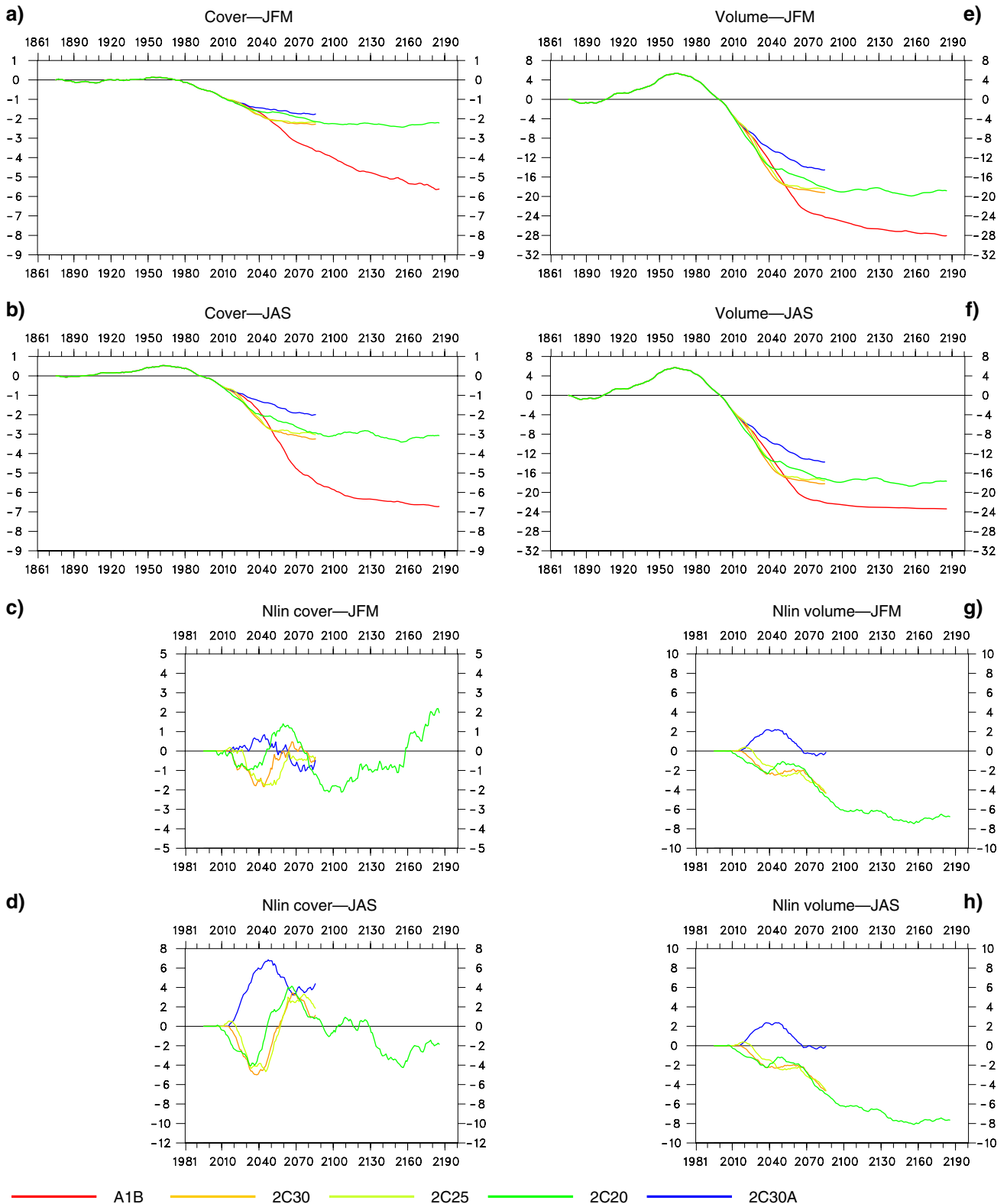


Fig. 5 Changes in the 30-year averages of seasonal mean sea-ice cover (a, b) and sea-ice volume (e, f) in the Arctic region with respect to the period 1861–1890 for January–March (JFM) and July–

September (JAS) and the nonlinear components of these changes (c, d, g, h) for the different experiments. Units are 10^6 km^2 (a, b), 10^5 km^2 (c, d), 10^3 km^3 (e, f) and 10^2 km^3 (g, h)

(JAS) by the end of the twenty-first century (Fig. 5e, f). Particularly in JAS, the sea-ice volume hardly decreases after the stabilization of the greenhouse gas concentrations in 2100, indicating that the continuing slow decrease in the sea-ice cover is compensated for by a slight increase in the thickness associated with the future increase in precipitation at high northern latitudes. AR4 does not give any estimates of the future changes in the sea-ice volume, but the changes simulated in A1B are at the upper limit of the different simulations contributing to AR4 (see below). The strong increase in particularly the sea-ice volume in the second half of the twentieth century is related to a multi-decadal variation with relatively low temperatures at high northern latitudes, causing a thickening of the sea-ice due to reduced melting. In late summer the relatively low temperatures also cause an increase in the sea-ice cover.

Also in the Antarctic region, A1B shows a considerable reduction of the sea-ice cover, i.e., by 2,169,000 km² (JFM) and 5,954,000 km² (JAS) by the end of the twenty-first century and by 2,736,000 km² (JFM) and 8,574,000 km² (JAS), respectively, by the end of the twenty-second century (Fig. 6a, b). The latter numbers correspond to a reduction by 65% in late austral winter but 87% in late austral summer (see Table 3). Hence, also in the Antarctic region the magnitude of the annual cycle of the sea-ice cover is enhanced in the future warmer climate, but to a somewhat lesser extent than in the Arctic region. In contrast to the Arctic region, the Antarctic sea-ice does not totally disappear in any year by the end of the twenty-second century. Again, AR4 gives very similar reductions of the sea-ice cover associated with the SRES A1B scenario by the end of the twenty-first century, i.e., about 2,500,000 km² in JFM and about 4,500,000 km² in JAS with respect to the period 1980–2000 (Meehl et al. 2007). Despite the markedly larger number given above, the agreement with AR4 is very good because the corresponding change (between the periods 1971–2000 and 2071–2100) simulated in A1B is 4,867,000 km² in JAS. The future changes in the Antarctic sea-ice volume are not presented here, because they by and large follow the changes in the sea-ice cover, because the sea-ice thickness is reduced to a similar extent over most of the area.

The numbers in AR4 that represent averages over simulations with 17 different coupled climate models, vary considerably between the individual models because of differences in the simulated response of the sea-ice to external forcings such as the increase in the atmospheric greenhouse gas concentrations (e.g., Flato et al. 2004). Arzel et al. (2006) presented the simulated changes in the annual mean sea-ice extent and volume between the periods 1981–2000 and 2081–2100 in response to the SRES

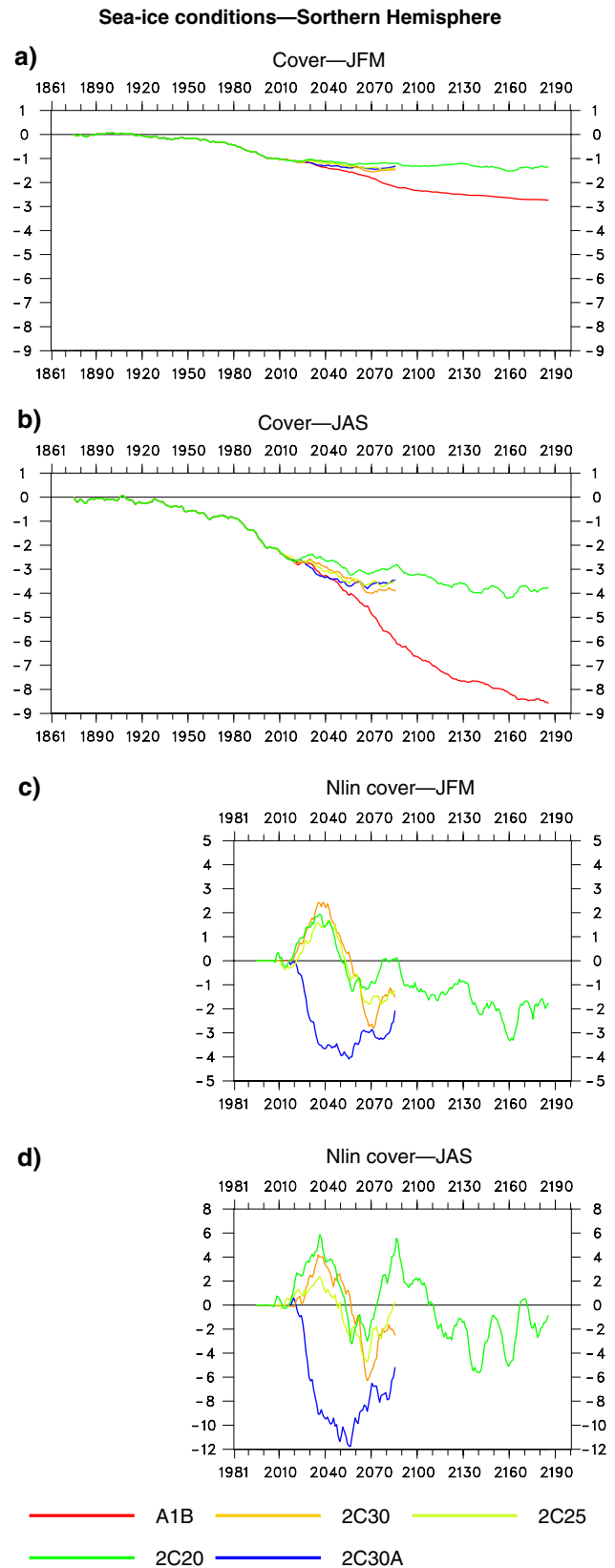


Fig. 6 As Fig. 5a–d, but for the Antarctic region

A1B scenario for 15 of the 17 different coupled climate models contributing to AR4. Although all models show future reductions of both the sea-ice extent and the sea-ice volume in both hemispheres, the magnitude of the changes varies considerably between the individual models. As for the Arctic region, the reductions in the sea-ice extent range approximately between 1,000,000 and 6,000,000 km² and the reductions in the sea-ice volume approximately between 5,000 and 25,000 km³. In the Antarctic region, the reductions in the sea-ice extent vary approximately between 2,000,000 and 6,000,000 km² and the reductions in the sea-ice volume approximately between 2,000 and 8,000 km³. The corresponding values for ECHAM5/MPI-OM (based on the periods 1971–2000 and 2071–2100) are close to the averages for the 15 models, except for the Arctic sea-ice volume, for which the model simulates a very strong reduction of more than 26,000 km³. This suggests that the sea-ice in the Arctic region simulated by ECHAM5/MPI-OM under present-day conditions is too thick while the sea-ice extent is simulated realistically (Jungclaus et al. 2006).

In 2C20 the reduction of the Arctic sea-ice cover is markedly weaker than in A1B, with 2,140,000 km² (JFM) and 2,935,000 km² (JAS) by the end of the twenty-first century and 2,216,000 km² (JFM) and 3,072,000 km² (JAS), respectively, by the end of the twenty-second century (Fig. 5a, b). The latter numbers correspond to reductions by 16% in late winter and by 43% in late summer (see Table 3). As for the sea-ice volume, the differences between 2C20 and A1B are less pronounced with reductions of 18,800 km³ (JFM) and 17,700 km³ (JAS) by the end of the twenty-second century in 2C20 (Fig. 5e, f), corresponding to reductions by 55% (JFM) and by 75% (JAS), respectively (see Table 3). As a consequence, the annual cycle of the sea-ice extent in the Arctic region is enhanced in 2C20, while the annual cycle of the sea-ice volume is slightly reduced. Also in the Antarctic region, 2C20 gives markedly smaller reductions in the sea-ice cover than A1B, with 1,352,000 km² in JFM and 3,769,000 km² in JAS at the end of the twenty-second century (Fig. 6a, b), corresponding to 43 and 29%, respectively, of the pre-industrial values (see Table 3). Hence, also in the Antarctic region the annual cycle in the sea-ice cover is enhanced in 2C20.

The nonlinear component of the changes in the Arctic sea-ice volume also illustrates the relatively strong reduction of the sea-ice volume, reaching –6,000 km³ in JFM and –8,000 km³ in JAS through most of the twenty-second century (Fig. 5g, h). This is roughly one-third of the overall reductions in 2C20. The nonlinear component of the Arctic sea-ice cover, on the other hand, varies around 0 through the twenty-second century, with negative values and (relatively strong reductions) through some periods and

positive ones (relatively weak reductions or increases) through others (Fig. 5c, d). These variations are presumably due to multi-decadal variations of the sea-ice cover caused by corresponding long-term variations in both the ocean and atmospheric circulation. 2C20 as well as 2C25 and 2C30 give relatively strong reductions in the Arctic sea-ice cover through the first few decades of the respective simulation in response to the strongly reduced sulphate aerosol load in these simulations, amplifying the future warming at high northern latitudes. This effect is most pronounced in late summer, with values exceeding –400,000 km² in JAS as compared to –100,000 km² in JFM. Apparently, the additional warming due to the reduction of the anthropogenic sulphate aerosol load is so strong that the near-surface temperatures reach above freezing in large parts of the Arctic region in late summer but not in late winter. This can also be seen from the nonlinear component of the Arctic sea-ice extent for 2C30A, exceeding 600,000 km² in JAS but only 80,000 km² in JFM. That is, the increased anthropogenic sulphate aerosol load in 2C30A results in a relatively weak reduction in the sea-ice extent, particularly in late summer. In contrast to this, the corresponding nonlinear component of the sea-ice volume does not show such a variation by season. In the Antarctic region, on the other hand, the increased sulphate aerosol load in 2C30A leads to a relatively strong reduction of 300,000 km² in JFM and of 1,000,000 km² in JAS (Fig. 6c, d). This is because the reduction in the sea-ice cover in 2C30A is as strong as in 2C30 (Fig. 6a, b) despite a reduction of the global warming by several tenths of a degree Celsius (see Fig. 1a).

The simulations presented here neither consider the second indirect effect of sulphate aerosols nor other kinds of aerosols such as black carbon or organic carbon. These may, however, have an effect on the sea-ice conditions, particularly in the Arctic region. The second indirect effect of sulphate aerosols, for instance, would weaken the reduction of the Arctic sea-ice cover even further because of a further reduction of the global warming (see above). The consideration of black aerosol, on the other hand, would considerably amplify the reduction of the Arctic sea-ice cover and volume because of an enhanced warming at high northern latitudes due to the albedo effect of black carbon deposited on the snow covering the Arctic sea-ice (Hansen et al. 2007).

4 Zonal mean changes

4.1 Near-surface variables

In this section, the changes in the zonal means of the annual mean values between the periods 2071–2100 and

1961–1990 are presented for some near-surface variables, considering four of the experiments (A1B, 2C20, 2C30, and 2C3A). Here, the recent period 1961–1990 is chosen as the reference period instead of the pre-industrial time period in order to allow for a better comparison of these changes with those presented in the scientific literature.

The future warming due to enhanced greenhouse gas concentrations is generally not equally distributed over the globe but more pronounced at high latitudes, in particular in the Northern Hemisphere (e.g., Meehl et al. 2007). This is also the case in the experiments shown here, with the warming at high northern latitudes exceeding 8°C for A1B and reaching 4°C in the other experiments (Fig. 7a). At other latitudes, 2C20 shows a warming at 2°C, except for the mid-latitudes in the Southern Hemisphere with a warming of 1°C. By this, the warming in 2C20 is generally about half as strong as for A1B. In 2C20, however, the warming is particularly strong at high northern latitudes as indicated by the nonlinear component of the near-surface temperature change in 2C20, reaching 0.5°C between 60 and 80°N (Fig. 7d). In the Southern Hemisphere, on the other hand, the warming at high latitudes is relatively weak in 2C20 with a nonlinear component between -0.2 and -0.3 °C. The higher anthropogenic sulphate aerosol load in 2C30A leads to a somewhat weaker warming than for 2C30 at all latitudes, with differences of 1°C at high northern latitudes and 0.5°C elsewhere (Fig. 7a). As indicated by the positive values of the corresponding nonlinear component, the warming at high latitudes is somewhat enhanced in 2C30A (Fig. 7d).

As a consequence of the warming, all experiments give a marked increase in daily precipitation in the tropics as well as at mid- and high latitudes of both hemispheres (Fig. 7b). In the Southern Hemisphere, precipitation is reduced in the entire subtropics, while in the Northern Hemisphere only 2C30A shows a slight decrease in the subtropics. All other experiments give a slight decrease at about 35°N, but none of the changes in the Northern Hemisphere subtropics are statistically significant. In A1B the changes are about twice as strong as in the other experiments, with increases of 0.7 mm/day in the tropics and 0.4 mm/day at mid- and high latitudes. 2C20 shows increases of 0.3 mm/day in the tropics and of 0.2 mm/day in the extratropics and a decrease of 0.1 mm/day in the Southern Hemisphere subtropics. 2C20 gives a relatively weak increase of daily precipitation at high southern latitudes and a relatively weak decrease in the Southern Hemisphere mid-latitudes, as indicated by the negative and positive values of the nonlinear component at the respective latitudes (Fig. 7e). Furthermore, 2C20 gives a relatively weak increase in the central tropics but rather strong increases at the southern and particularly at the northern edge of the tropics. The higher anthropogenic sulphate aerosol load in 2C30A leads to weaker increases

of daily precipitation in the tropics and in the extratropics in both hemispheres as compared to 2C30. Furthermore 2C30A gives a slight decrease in the Northern Hemisphere subtropics, where 2C30 shows a slight increase (Fig. 7b). This is also indicated by the negative values of the corresponding nonlinear component of the change in daily precipitation with negative values at respective latitudes (Fig. 7e). Similar to 2C20, 2C30A gives a relatively weak increase of daily precipitation in the central tropics but rather strong increases at the southern and particularly at the northern edge of the tropics

All experiments show a decrease of the sea-level pressure in part of the mid-latitudes and at high latitudes of both hemispheres, i.e., north and south of 50°N and 55°S, respectively (Fig. 7c). By this, the future changes in the sea-level pressure indicate a marked amplification of the pressure gradient between mid- and high latitudes, particularly in the Southern Hemisphere, despite a decrease in the meridional near-surface temperature gradient (see Fig. 7a). In A1B the decrease in the Antarctic region is about twice as strong as in the Arctic region, but for 2C20 the corresponding changes have a similar magnitude in both hemispheres. In the Southern Hemisphere extratropics the sea-level pressure is significantly increased, particularly in A1B, while in the Northern Hemisphere such an increase is hardly visible. 2C20 gives rather weak changes of the sea-level pressure at high and mid-latitudes of the Southern Hemisphere, i.e., a relatively weak pressure decrease (increase) at high (mid-) latitudes, indicated by the negative (positive) values of the nonlinear component of sea-level pressure change in 2C20 at the respective latitudes (Fig. 7f). At high latitudes the nonlinear component reaches a maximum value of 1 hPa. As for the impact of the higher anthropogenic sulphate aerosol load, the only marked difference between 2C30A and 2C30 is the somewhat weaker decrease of the sea-level pressure in the Arctic region (Fig. 7c), which can also be identified in the nonlinear component of the corresponding change (Fig. 7f). The negative values of -0.5 hPa indicate a relatively strong pressure decrease in the Antarctic region in 2C30A.

4.2 Latitude–height cross sections

In this section, latitude–height cross sections for the annual mean temperature and zonal wind component are presented, i.e., the changes between the periods 2071–2100 and 1961–1990 for A1B and 2C20 as well as the differences between A1B and 2C20 and between 2C30A and 2C30, respectively, for the period 2071–2100. The period 1961–1990 represents the present-day climate (“pre”) and the period 2071–2100 the future climate (“fut”).

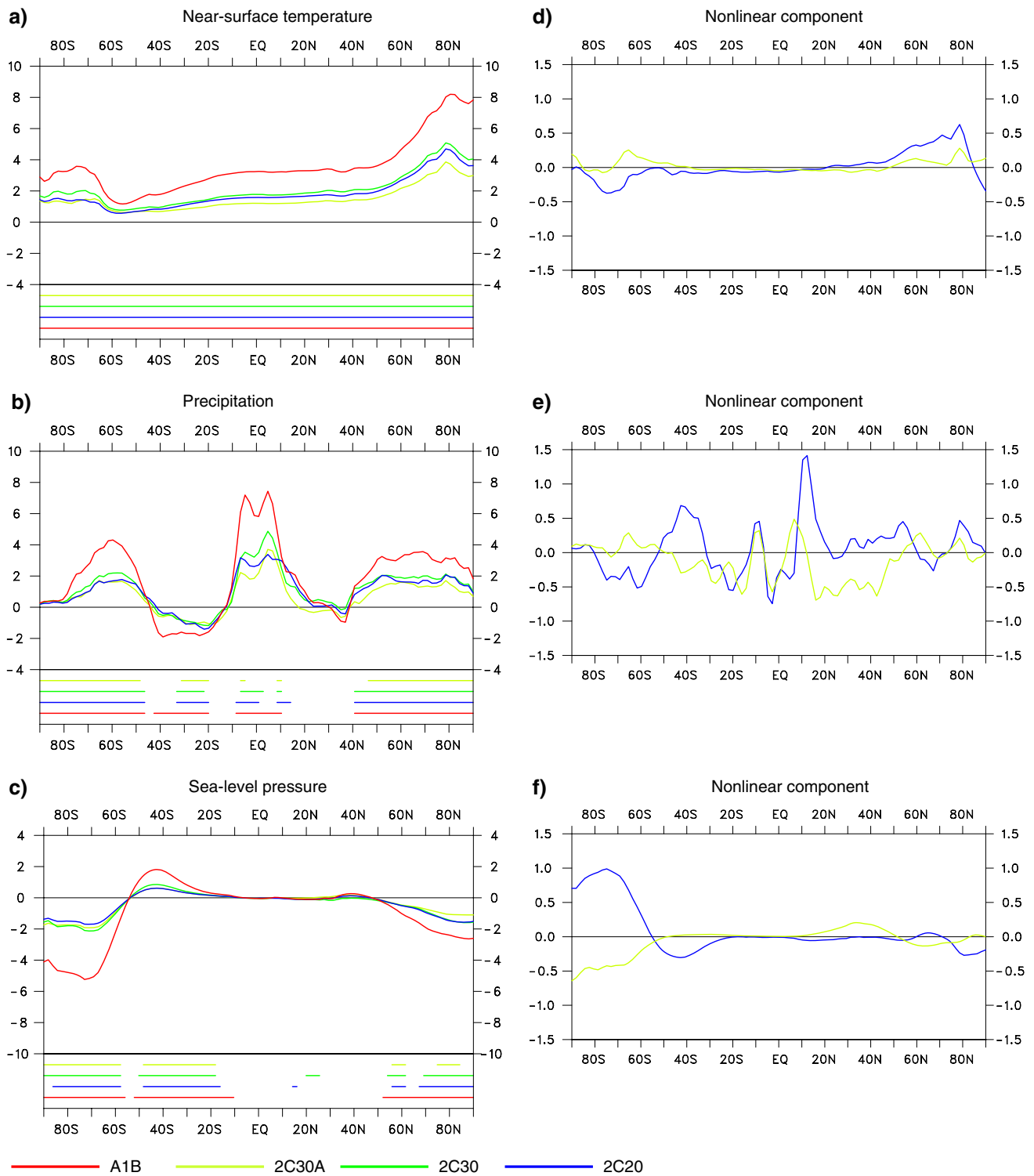


Fig. 7 Changes in the annual mean zonal means between the periods 1961–1990 and 2071–2100 for the annual means of **a** the near-surface temperature, **b** daily precipitation, and **c** sea-level pressure for A1B, 2C30, 2C30A and 2C20. The significance of these changes at the

99.0% level (**a**, **b**) and the 97.5% level (**c**) is indicated by the *horizontal lines*. Furthermore, the nonlinear components of the changes in 2C20 and 2C30A are shown (**d–f**). Units are °C (**a**, **d**), 1/10 mm/day (**b**, **e**), and hPa (**c**, **f**)

For the future, both A1B and 2C20 show a warming in the troposphere and a cooling in the stratosphere, particularly at high latitudes (Fig. 8a, b). The strongest warming

with more than 6°C in A1B and more than 3°C in 2C20, respectively, occurs in two areas, the upper troposphere in the tropical region and the lower troposphere in the Arctic

region. The weakest warming with less than 2°C in A1B and less than 1°C for 2C20 occurs over the oceans in the Southern Hemisphere in the lower and mid-troposphere. By this, the future changes simulated in these two experiments correspond very well to the respective changes in AR4 representing the average for several different coupled climate models (Meehl et al. 2007). The aforementioned changes in the temperature distribution lead to a strengthening of the meridional temperature gradient between the tropical upper troposphere and the lower stratosphere in the extratropics in both hemispheres. In the Northern Hemisphere, the meridional temperature gradient is markedly reduced in the lower troposphere but is enhanced throughout the troposphere in the Southern Hemisphere. The differences between A1B and 2C20 for the period 2071–2100 have a very similar structure as the future changes simulated in 2C20 (Fig. 8c). They are, however, generally stronger than the future changes in 2C20, with the exception of the lower troposphere in the Arctic region, where 2C20 gives a maximum warming of more than 3°C for the entire area north of 60°N (Fig. 8c).

Consistent with the weaker global warming due to the higher anthropogenic sulphate aerosol load, 2C30A gives a

weaker warming than 2C30 throughout the troposphere as well as a slightly weaker cooling in the upper stratosphere except for the Arctic region (Fig. 8d). In the lower and mid-troposphere of the Northern Hemisphere, the differences are about twice as large as in the Southern Hemisphere, indicating that the higher sulphate aerosol load leads to a more pronounced cooling in the Northern Hemisphere than in the Southern Hemisphere. This is due to the relatively large sulphate aerosol concentrations in the Northern Hemisphere extratropics. At high latitudes, 2C30A also gives a cooling through most of the stratosphere, exceeding -1.0°C in the Southern Hemisphere and reaching between -0.25 and -0.50°C in the Northern Hemisphere. This cooling is caused by the lower stratospheric ozone concentrations at high latitudes in 2C30A, i.e., about 300 ppb in the Southern and about 140 ppb in the Northern Hemisphere. By this, the effect of lower stratospheric ozone level overrules the effect of the enhanced sulphate aerosol load, which leads to a warming in the stratosphere due to the tropospheric cooling.

As a consequence of the strengthening of the meridional temperature gradient between the tropical upper troposphere and the lower stratosphere in the extratropics, both

Temperature

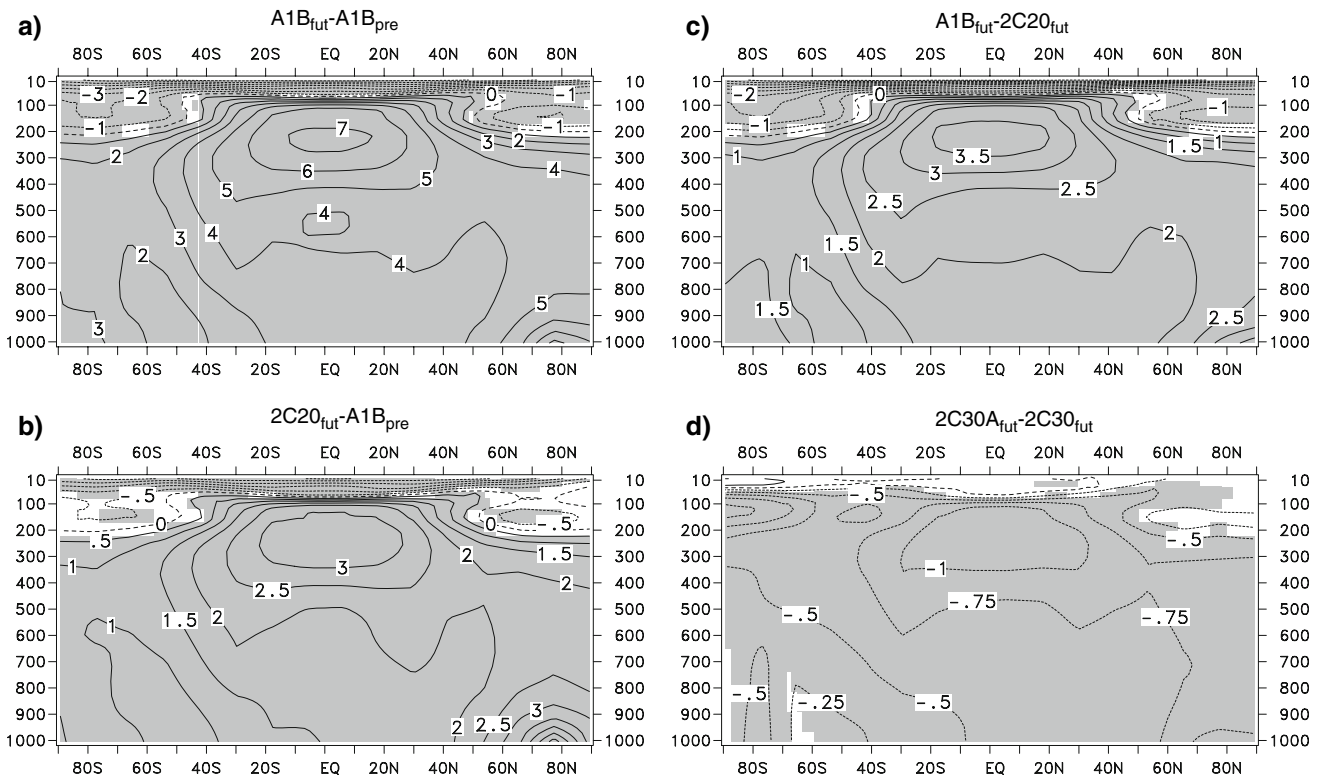


Fig. 8 Changes in the annual mean zonal means of temperature between the periods 1961–1990 and 2071–2100 for **a** A1B, **b** 2C20 as well as the differences, **c** between A1B and 2C20, and **d** between 2C30A and 2C30 for the period 2071–2100 in both cases. The

significance of these changes at the 99.0% level (**a–c**) and the 97.5% level (**d**) is indicated by the shading. Units are $^{\circ}\text{C}$, the contour interval is 1°C (**a**), 0.5°C (**b**, **c**), and 0.25°C (**d**)

A1B and 2C20 show marked increases in the westerly winds in the stratosphere between 20 and 60° northern and southern latitude, respectively (Fig. 9a, b), leading to an upward extension of the zone with relatively strong westerly winds into the stratosphere. Furthermore, the westerly winds intensify throughout the troposphere in the Southern Hemisphere extratropics, so that the zone of relatively strong westerly winds is extended further southward. In the tropics, on the other hand, the two experiments show a slight (hardly significant) weakening of the easterly winds throughout the troposphere. Consistent with the larger magnitude of the temperature differences between A1B and 2C20 for the period 2071–2100 compared to the future changes simulated in 2C20, also the corresponding differences in the zonal wind component are somewhat larger (Fig. 9c). This is particularly the case in the Southern Hemisphere, where the differences between A1B and 2C20 are about twice as large as the future change simulated in 2C20.

The enhanced anthropogenic sulphate aerosol load in 2C30A has only minor effects on the zonal wind component in the troposphere, although the differences between 2C30A and 2C30 show some of the typical features related to the weaker global warming in 2C30A (Fig. 9d). In the

stratosphere, on the other hand, the westerly winds are reduced roughly between 50°S and 60°N in 2C30A, consistent with the reduced meridional temperature gradient in the stratosphere due to the lower stratospheric ozone levels (see Fig. 8d). Again, the differences in the stratosphere indicate that the local effect of the reduced stratospheric ozone levels is more important than the remote effect of enhanced sulphate aerosol load.

5 Local changes

Also for the local changes in climate the recent period 1961–1990 is chosen as the reference period, again, in order to allow for a better comparison of these changes with those presented in the scientific literature.

5.1 Sea-ice conditions

Consistent with the previous discussion of the sea-ice conditions, seasonal means for the periods January–March (“JFM”) and July–September (“JAS”) are considered for the local changes in the sea-ice conditions. Again, only

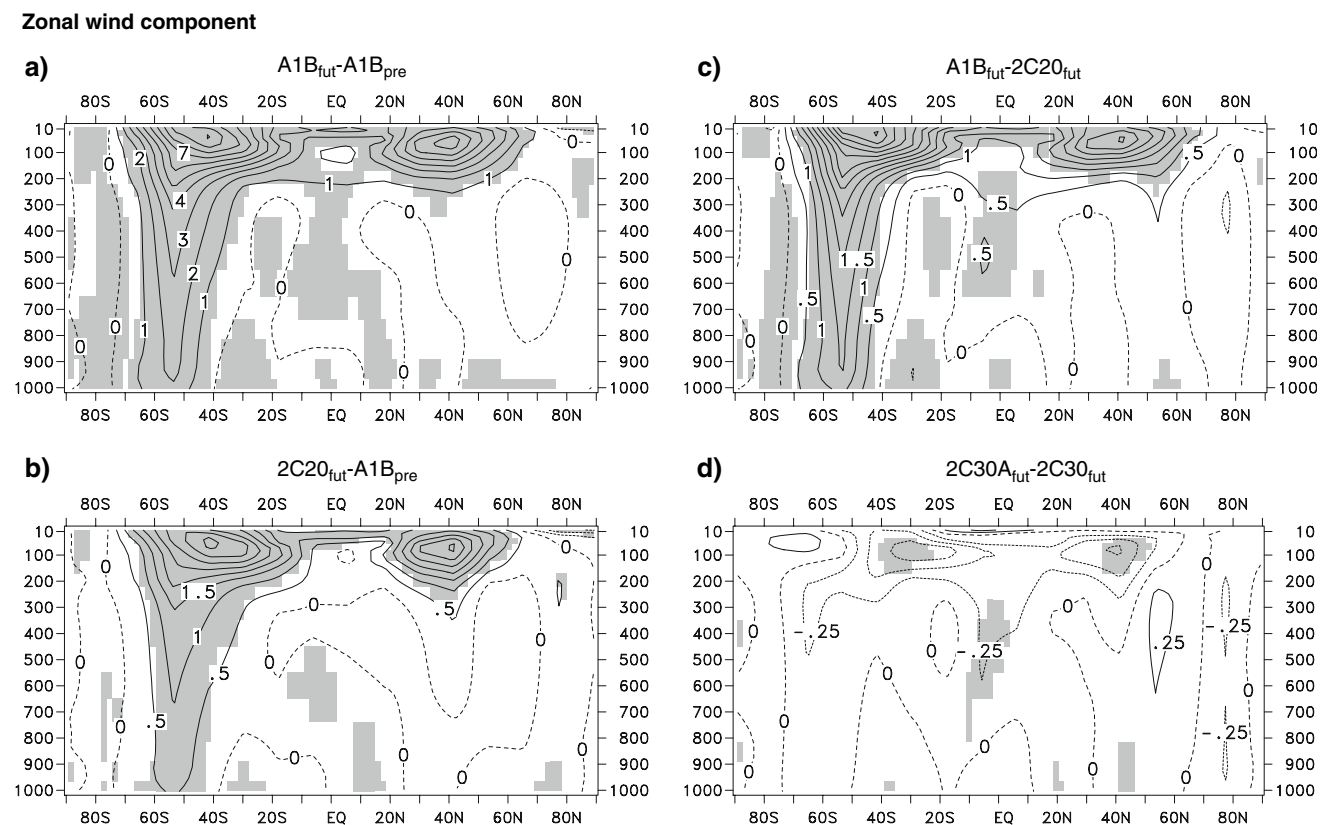


Fig. 9 As Fig. 8, but for the zonal wind component. The significance levels are at 97.5% (a–c) and at 95% (d). Units are m/s, the contour interval is 1 m/s (a), 0.5 m/s (b, c), and 0.25 m/s (d)

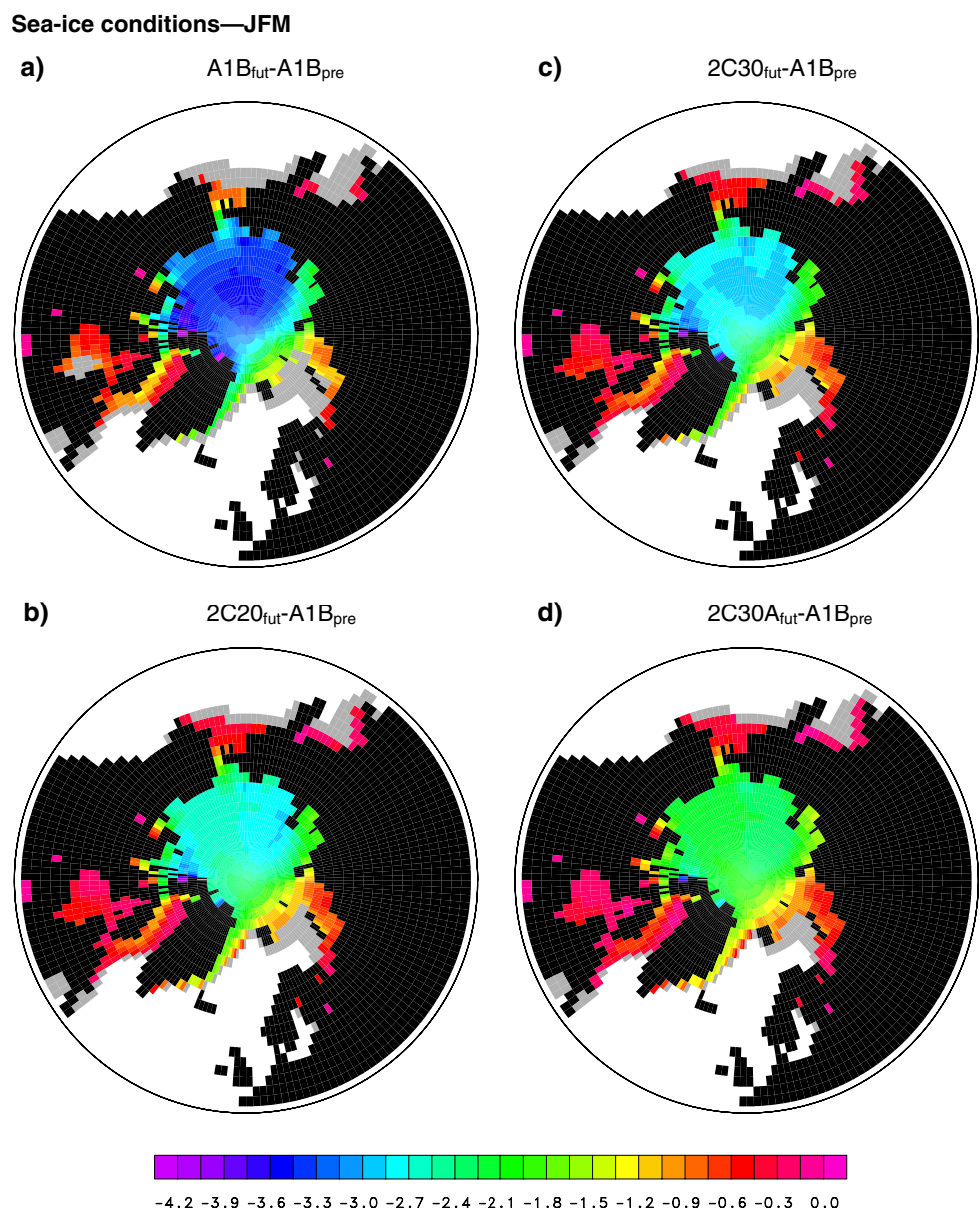
grid-boxes with at least 15% of the area covered by sea-ice are included, following a widely used practice in observational studies (e.g., Johannessen et al. 2004).

In late winter, all experiments show a reduction in both the sea-ice cover and the sea-ice thickness due to the increased greenhouse gas emissions in the Arctic region (Fig. 10). The sea-ice has particularly retreated in the Barents Sea, the Sea of Okhotsk and the Bering Sea, while the sea-ice thickness is most markedly reduced in the East Siberian Sea and the Beaufort Sea. The magnitude of the reduction follows by and large the magnitude of the global warming, with the largest reductions in A1B (Fig. 10a) and the smallest ones in 2C30A (Fig. 10d). In A1B, for instance, the sea-ice thickness is reduced by about 3.5 m in a large part of the Arctic region compared to about 2 m in

2C30A. Moreover, the shrinking of the sea-ice cover in the most sensitive areas, i.e., the Barents Sea, the Sea of Okhotsk and the Bering Sea, is strongest in A1B and weakest in 2C30A. In 2C20 the sea-ice thickness is reduced by about 2.5 m in a large part of the Arctic region, as compared to 3.5 m in A1B, and the reduction of the sea-ice cover is generally, that is all along the edge of the sea-ice, less pronounced (Fig. 10b). In JFM, the main effect of the higher anthropogenic sulphate aerosol load in 2C30A is a weaker thinning of the sea-ice, while the reduction of the sea-ice cover is very similar to 2C30 (Fig. 10c).

In late summer, all experiments show a markedly stronger reduction in both the sea-ice extent and the sea-ice thickness in the Arctic region than in late winter (Fig. 11). In all experiments the sea-ice cover has disappeared in the

Fig. 10 Changes in the 30-year averages of JFM mean sea-ice cover and sea-ice thickness between the periods 1961–1990 (“pre”) and 2071–2100 (“fut”) for **a** A1B, **b** 2C20, **c** 2C30 and **d** 2C30A. Marked in *grey* are those areas that are covered with sea-ice only during 1961–1990 and in the *other colours* are those areas that are covered with sea-ice during both periods. Units are m for the sea-ice thickness



Barents Sea and the Kara Sea as well as in the Fox Basin and the Baffin Bay. In A1B, the sea-ice cover has also disappeared in the Chukchi Sea, the southern part of the Beaufort Sea and the Laptev Sea (Fig. 11a). Moreover, the sea-ice has disappeared on the eastern coast of Greenland. In 2C20 all these areas are still covered with sea-ice (Fig. 11b), so that the ice-albedo-feedback is considerably weaker than in A1B. In contrast to JFM, the higher anthropogenic sulphate aerosol load in 2C30A has also an effect on the sea-ice cover, with a markedly smaller retreat all along the edge of the sea-ice (Fig. 11d). The sea-ice thickness is not only markedly reduced in the East Siberian Sea and the Beaufort Sea but also in the area north of the Canadian Archipelago, i.e., by about 3 m in 2C20 and about 2 m in 2C30A.

Also in the Antarctic region, all experiments show a reduction in both the sea-ice cover and the sea-ice thickness due to the increased greenhouse gas emissions in both seasons (Fig. 12). The sea-ice has particularly retreated in the Amundsen Sea and the Wedell Sea, and the sea-ice thickness is mostly reduced in the Wedell Sea. In contrast to the Arctic region, the magnitude of the reduction follows the magnitude of the global warming only when the relatively strong A1B scenario is compared to the relatively weak scenarios (2C20, 2C30 and 2C30A). The differences between the three weaker scenarios, on the other hand, are very small despite the differences in the respective changes of the global mean temperatures, particularly in 2C30A. Therefore, the changes in the sea-ice conditions in 2C30 and 2C30A are not presented here. In JFM, the sea-ice is retreated almost

Fig. 11 As Fig. 10, but for JAS

Sea-ice conditions—JAS

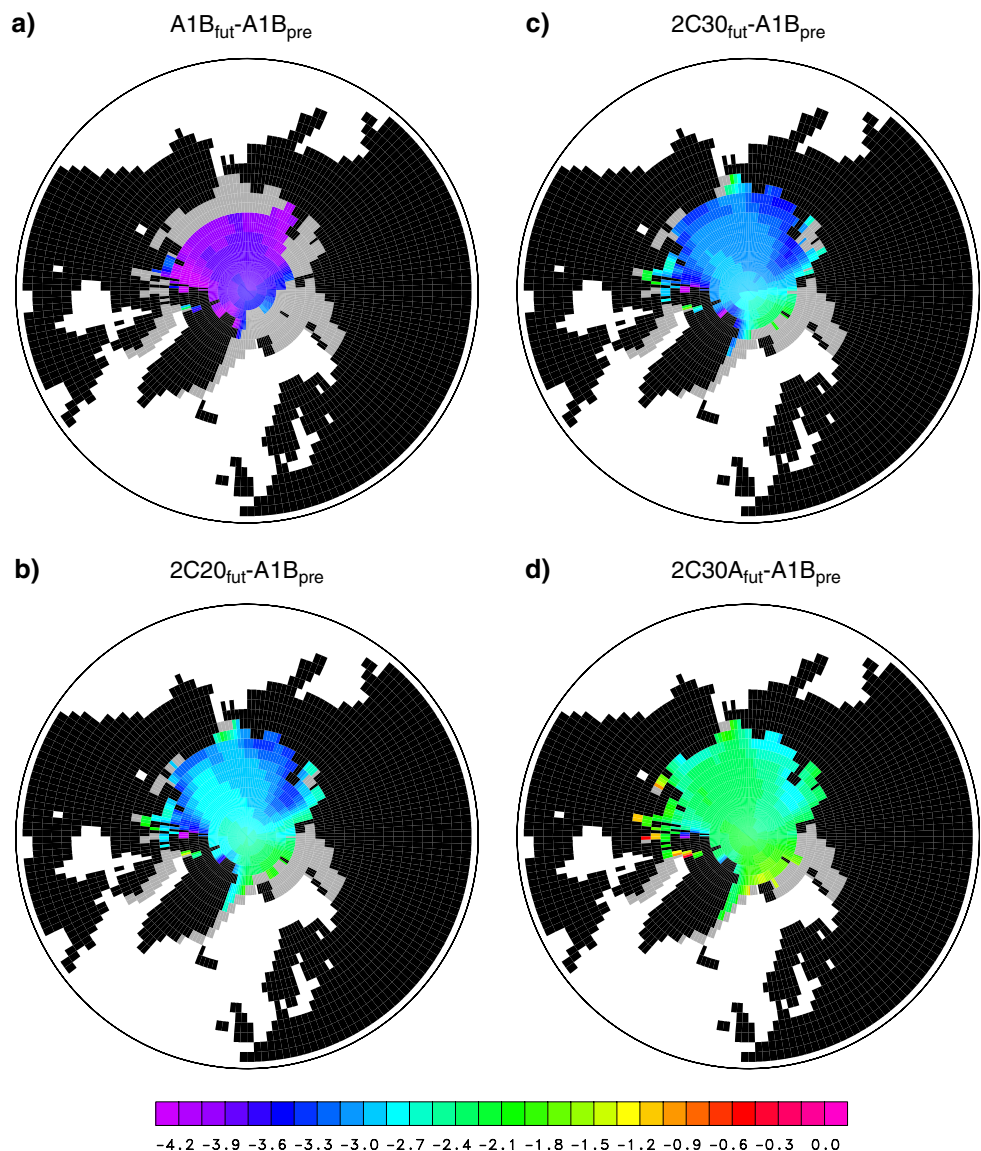
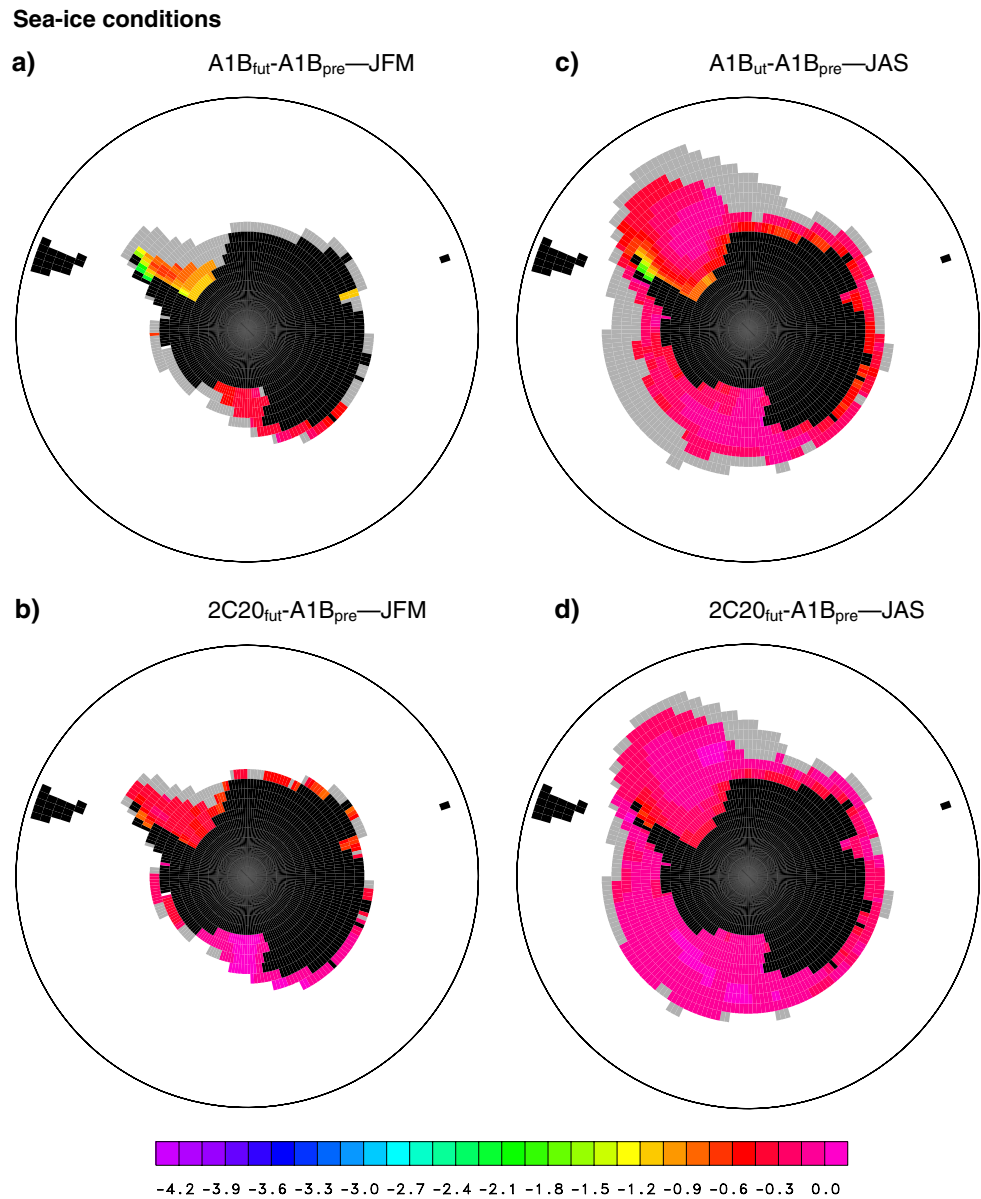


Fig. 12 Changes in the 30-year averages of seasonal mean sea-ice cover and sea-ice thickness between the periods 1961–1990 and 2071–2100 for **a, c** A1B and **b, d** 2C20 for JFM and JAS, respectively. Marked in *grey* are those areas that are covered with sea-ice only during 1961–1990 and in the *other colours* are those areas that are covered with sea-ice during both periods. Units are m for the sea-ice thickness



everywhere around Antarctica in A1B (Fig. 12a) but only in the Wedell Sea and a few smaller areas around Antarctica in 2C20 (Fig. 12b). In the Wedell Sea, for instance, the sea-ice thickness is reduced by about 1 m in A1B but only by about 50 cm in 2C20. In JAS, the differences between these two simulations are not as pronounced for the sea-ice thickness, with reductions of about 40 cm (A1B; Fig. 12c) and about 20 cm (2C20; Fig. 12d) in most of the Arctic region. The sea-ice cover, on the other hand, is markedly more reduced in A1B, particularly in the Amundsen Sea.

A comparison with the local changes in the sea-ice conditions for the SRES A1B scenario presented in AR4 shows very similar changes in the sea-ice extent by the end of the twenty-first century (2080–2100; Meehl et al. 2007). In late summer, for instance, the Arctic sea-ice has

retreated from most coastlines except for the Canadian Archipelago and northern Greenland. In late austral summer, on the other hand, the Antarctic sea-ice is disappeared in the Amundsen Sea and retreated considerably in the Wedell Sea. The changes in the sea-ice conditions in AR4 represent averages over simulations with a number of different coupled climate models, which vary considerably between the different models (e.g., Flato et al. 2004). Arzel et al. (2006) did, however, not present the local changes in the sea-ice conditions for the different models contributing to AR4. As for the area averages, the ECHAM5/MPI-OM coupled climate model is close to the average of the various models considered, except for the sea-ice thickness in the Arctic region, which is simulated too thick in ECHAM5/MPI-OM.

5.2 Near-surface temperature

A1B shows a pronounced warming due to the increased greenhouse gas concentrations in the Arctic region, exceeding 6°C over most of the area but reaching more than 12°C over the Barents Sea and the Kara Sea (Fig. 13a). This strong warming is related to the positive ice-albedo-feedback in the Arctic region as a consequence of the retreating

sea-ice (see Figs. 10a, 11a). Particularly in the Barents Sea and the Kara Sea, the simulations show a strong retreat of the sea-ice, most pronounced in late summer. The ice-albedo-feedback is also the reason for the relatively strong warming over the Ross Sea, the Amundsen Sea and the Weddell Sea in the Antarctic region. Except for the high latitudes, the warming is stronger over the land areas, generally exceeding 4°C, than over the adjacent ocean

Near-surface temperature

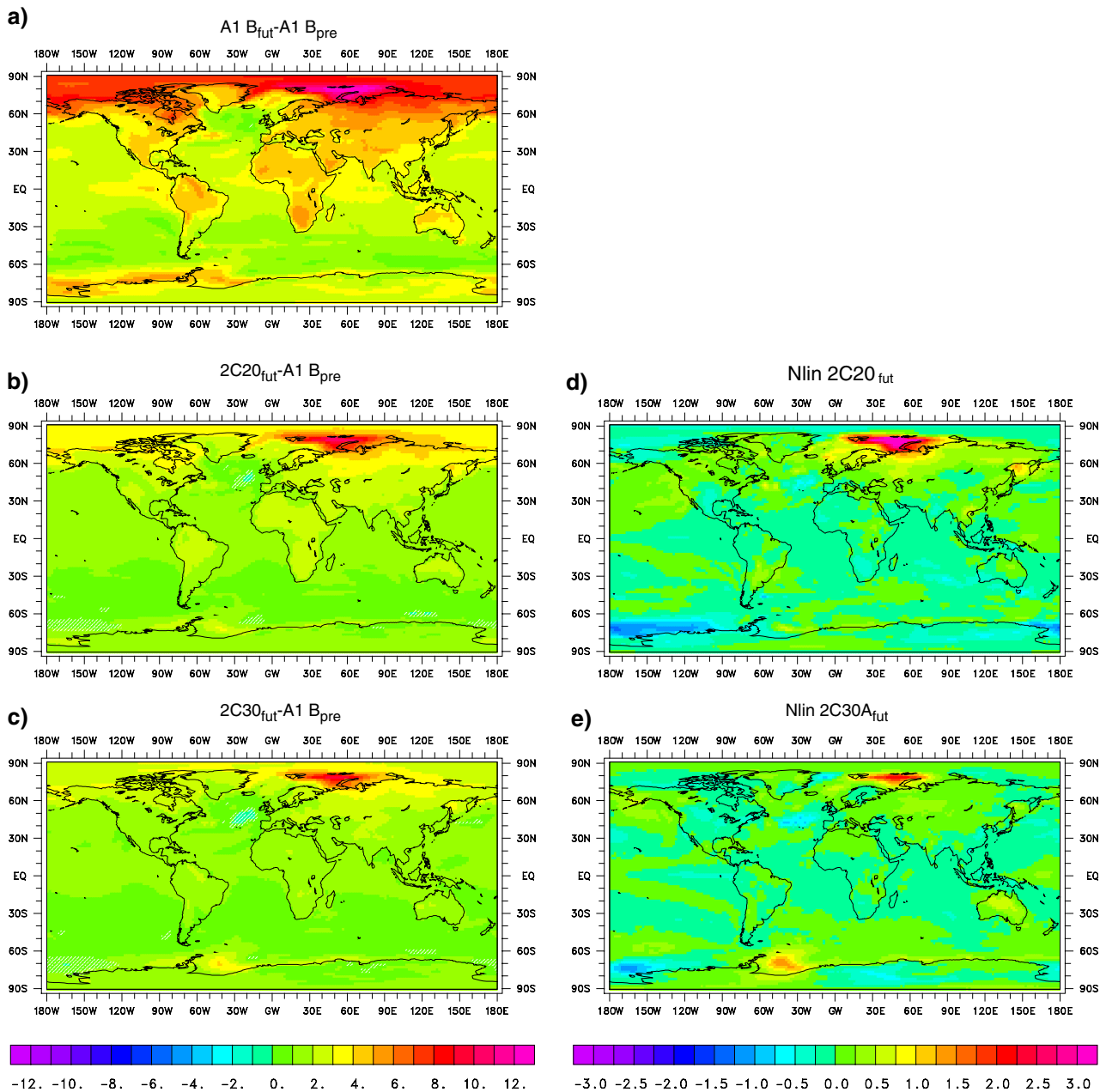


Fig. 13 Changes in the annual mean near-surface temperature between the periods 1961–1990 and 2071–2100 for **a** A1B, **b** 2C20 and **c** 2C30A as well as the nonlinear components of **d** 2C20 and **e** 2C30A for the period 2071–2100. In **a–c** the areas where these

changes are not significant at the 99.0% level are marked by the *white stippling*. Units are °C, the contour interval is 1°C (**a–c**) and 0.25°C (**d, e**)

basins due to higher heat capacity of the oceans. In northern Canada and in northern Russia the warming is further enhanced by the positive snow-albedo-feedback as a consequence of the shortened period with snow at the ground. As for the oceans, A1B shows a pronounced warming in the eastern tropical Pacific Ocean, similar to the SST anomaly during an El Niño event, and a very small warming in the Atlantic Ocean, roughly between the southern tip of Greenland and the British Isles, as well as in the Southern Ocean. The latter is related to the strong vertical mixing of the water masses in these ocean basins.

By this, A1B has the main features in common with the average response to the SRES A1B scenario for numerous coupled climate models contributing to AR4 (Meehl et al. 2007). There are, however, some regional differences. A1B gives, for instance, a very weak warming in the Atlantic Ocean to the west of the British Isles. Furthermore, the warming in the Arctic region is particularly strong in A1B, partly because of relatively low temperatures at high northern latitudes during the second half of the twentieth century due to a multi-decadal variation in the coupled atmosphere–ocean system. The El Niño like warming pattern in the eastern tropical Pacific Ocean, on the other hand, is a common feature of most climate change simulations with the different coupled climate models (Yamaguchi and Noda 2006).

2C20 (Fig. 13b) shows a similar pattern of the future change in the near-surface temperature, but the magnitude is about half as strong as for A1B. However, the warming over the Barents Sea and the Kara Sea is relatively strong, exceeding 8°C, which is more than half of the 12–14°C for A1B in this region. 2C20 does not show a pronounced El Niño like warming pattern in the eastern tropical Pacific Ocean as A1B but a uniform warming over the entire tropical Pacific. Apparently, the El Niño like warming pattern does not emerge before the greenhouse gas forcing has reached a particular strength. In the Atlantic west of the British Isles, 2C20 shows a slight (nonsignificant, though) cooling, and over the Ross Sea and the Amundsen Sea the warming is relatively weak in 2C20. These differences between 2C20 and A1B can also be seen in the distribution of the nonlinear component of the changes in 2C20 (Fig. 13d). The positive anomalies of more than 3°C over the Barents Sea and the Kara Sea indicate the particularly strong warming in this region in 2C20, while the negative ones over the Ross Sea and the Amundsen Sea indicate the particularly weak warming in the region. The relatively strong warming over the Barents Sea and the Kara Sea extends into Siberia as well as into northern and eastern Europe. The distribution shows a tongue of negative anomalies centred on the equator in the eastern Pacific Ocean, indicating that the El Niño like warming pattern has not come up in 2C20. As a consequence, 2C20 gives a

relatively strong warming over the southern and northern Pacific (e.g., Trenberth et al. 2002). The negative anomalies in the tropical Pacific Ocean are part of a general pattern with a less pronounced warming also in the tropical Atlantic Ocean and Indian Ocean as well as partly over the adjacent continents, which, again, is related to the fact that the El Niño like warming pattern does not emerge in 2C20.

Except for the relatively strong warming over the Barents Sea and the Kara Sea, the warming in 2C20 is very similar to the temperature difference between 2000 and 2100 for the 2°C scenario in Hansen et al. (2007), with a global warming of 1.42°C. The Alternative scenario, on the other hand, gives considerably weaker warming in all regions, consistent with the relatively weak global warming of 0.66°C. In the Arctic region the Alternative scenario gives a future warming between 1 and 2°C. The twentieth century stabilization scenario with CCSM3 in Meehl et al. (2005), on the other hand, gives already a warming of the temperatures in the Arctic region by about 3°C similar to 2C20. Moreover, the B1 scenario with PCM gives a slightly stronger warming in the Arctic region than 2C20, except for the area including the Barents Sea and the Kara Sea.

2C30A shows a similar pattern of the future change in the near-surface temperature as 2C20 but with a somewhat weaker magnitude (Fig. 13c). In the Arctic region, for instance, the temperature increase is about 1°C weaker than in 2C20, and this is also the case over most of the land areas. This shows that the higher anthropogenic sulphate aerosol load in 2C30A leads to a general reduction of the future warming, in association with the direct and the first indirect of the sulphate aerosols. As indicated by the nonlinear component of the changes in 2C30A, 2C30A gives a relatively strong warming over the Barents Sea in the Arctic and over the Ross Sea in the Antarctic region (Fig. 13e). A relatively weak warming indicated by the negative anomalies, on the other hand, is found over North America, the North Atlantic and the western part of the North Pacific, namely in the vicinity of the industrialized areas at Northern Hemisphere mid-latitudes with a strong production of sulphate aerosols. Similar to the nonlinear component of the changes in 2C20, the El Niño like warming pattern in the eastern tropical Pacific Ocean is less pronounced in 2C30A than in 2C30, associated with a weaker warming in the tropical Atlantic Ocean and Indian Ocean.

The relatively weak warming in 2C30A would be even more reduced if also the second indirect effect of sulphate aerosols was considered in the ECHAM5 AGCM (e.g., Rotstayn and Penner 2001). Moreover would changes in the concentrations of other kinds of aerosols affect the future warming, first via the direct radiative effects but also via indirect effects. Based on the estimates of the radiative

forcing of these two kinds of aerosols in Schulz et al. (2006), a higher load of carbonaceous aerosols would further reduce the future warming while a higher load of black carbon would increase the future warming. The latter is particularly true at high latitudes because of the albedo effect of black carbon deposited on the snow covering the Arctic sea-ice as well as the land areas in the northern parts of North America and Russia (Hansen et al. 2007).

5.3 Regional example: Greenland

As for the area around Greenland, 2C20 shows an increase in the annual mean temperature of more than 2°C with respect to present-day conditions over most of the region. In the northeastern part of the area the future warming actually reaches the threshold of 2.7°C, suggested by Gregory et al. (2004a, b) as the temperature change at which the Greenland ice-sheet starts to melt. Since the ice-sheet is mostly sensitive to the warming in summer and early autumn but not in winter, when no melting takes place, the changes in the near-surface temperature during summer give an indication of the future changes of the Greenland ice-sheet. Further, the changes with respect to pre-industrial times, here represented by the period 1861–1890, should be considered. During summer (June–August; “JJA”), 2C20 shows a somewhat stronger warming over Greenland (between 0.3 and 0.5°C) than for the annual average but a somewhat weaker warming over the surrounding ocean areas except to the east of Greenland (Fig. 14). This is because the sea-ice disappears in this region during summer, while there generally is no sea-ice west of Greenland already for pre-industrial conditions and there still is sea-ice north of Greenland in the future. The somewhat stronger warming over Greenland compared to the annual average, on the other hand, is a consequence of the lower surface albedo in summer with less fresh snow on the ice-sheet than in the other seasons. In summer, the warming of the near-surface temperature exceeds 2.5°C over more than half of Greenland and 3.0°C in the northeastern part. By this, the future warming in 2C20 is still below the threshold of 2.7°C when Greenland as a whole is considered, but in the northeastern part of Greenland this threshold is clearly exceeded, indicating melting of this part of the Greenland ice-sheet already under the 2°C-stabilization scenario.

The warming in the area around Greenland is just one prominent example of regional climate changes that can have wide-reaching consequences because of the potential loss of the Greenland ice-sheet (Huybrechts et al. 1991; Gregory et al. 2004a, b). There are other examples of vulnerabilities in the climate system but also of vulnerabilities for ecosystems and biodiversity, of vulnerabilities

Near-surface temperature—JJA

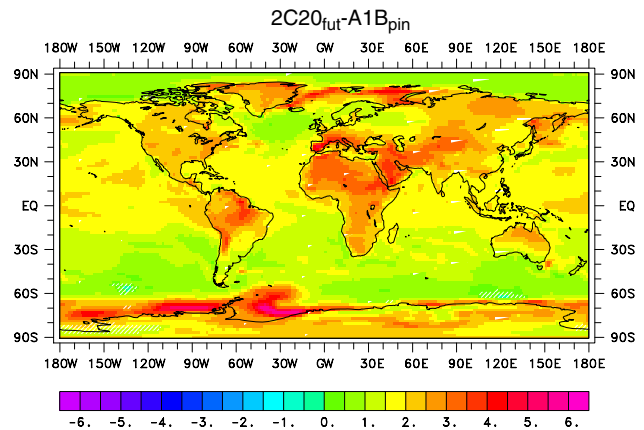


Fig. 14 Changes in the summer (June–August; “JJA”) mean near-surface temperature between the periods 1861–1890 (“pin”) and 2071–2100 for 2C20. The areas where these changes are not significant at the 99.0% level are marked by the white stippling. Units are °C, the contour interval is 0.5°C

for water resources, agriculture and food as well as of climate change impacts in various sensitive areas of the globe (Schellnhuber et al. 2006) that are worthwhile to consider. This would, however, be beyond the scope of this study. Another interesting issue regarding regional climate changes would be to investigate whether and, if so, how the relative importance of the regional climate change hot spots as defined in Giorgi (2006) changes under the relatively weak 2°C stabilization scenario.

5.4 Precipitation

As for daily precipitation, A1B shows an increase in the tropics and at mid- and high latitudes and a reduction in the subtropics (Fig. 15a). The changes in the tropical and subtropical regions are caused by the enhanced convergence of the large-scale flow and intensified upward motions with more precipitation in the tropics causing, in turn, intensified downward motions with less precipitation in the subtropics. The increases at mid- and high latitudes, on the other hand, are due to an increase in the precipitation intensity within low-pressure systems as a consequence of the generally enhanced atmospheric moisture content in the future. The most pronounced increase occurs over the tropical Pacific Ocean in association with the El Niño like warming pattern in this ocean basin (see Fig. 13a). This increase in precipitation is accompanied by decreases over Indonesia, the subtropical parts of the Pacific Ocean and Central America. These changes in daily precipitation are similar to the average response to the SRES A1B scenario for numerous coupled climate models contributing to AR4 (Meehl et al. 2007). In particular, the areas with significant

Precipitation

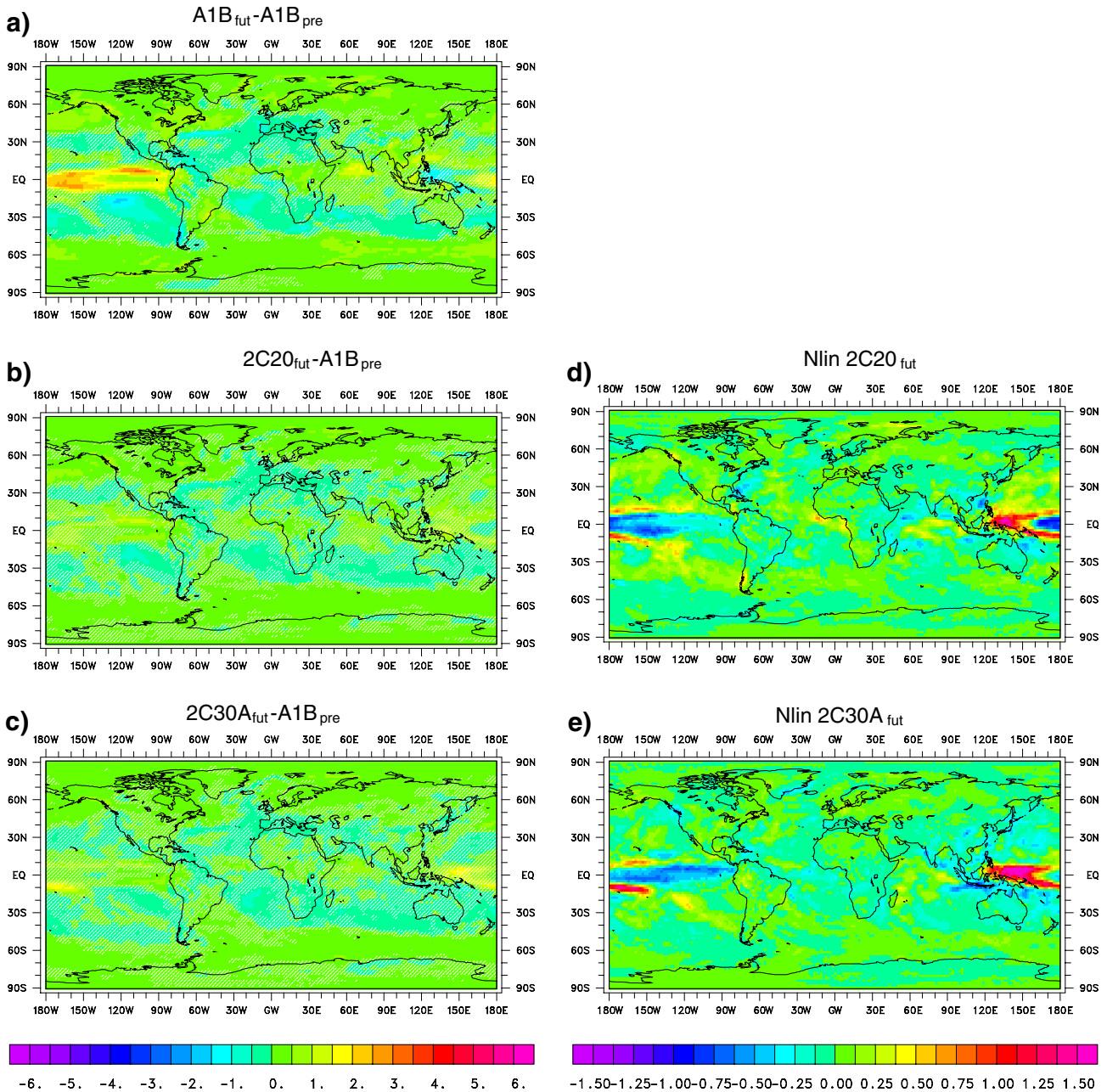


Fig. 15 As Fig. 13, but for daily precipitation. The significance level is at 95% (a–c). Units are mm/day, the contour interval is 0.5 mm/day (a–c) and 0.125 mm/day (d, e)

changes in A1B coincide with those areas, where at least 80% of the models contributing to AR4 agree on the sign of the future changes in daily precipitation.

In 2C20 (Fig. 15b) the future changes in daily precipitation have a similar structure as in A1B, but the magnitude of the changes is generally about half as strong as in A1B. The increase over the tropical Pacific Ocean, however, is less pronounced in 2C20 due to the less pronounced El Niño like warming pattern in this

experiment (see Fig. 13b). In contrast to A1B, precipitation is actually enhanced over the western Pacific and Indonesia. The differences over the tropical Pacific are also the most pronounced feature of the nonlinear component of the changes in 2C20 (Fig. 15d). The negative anomalies over the eastern and central tropical Pacific Ocean indicate a weak increase in the region with enhanced precipitation during an El Niño event, while the positive anomalies over the western tropical Pacific Ocean

and Indonesia illustrate an increase in the region with reduced precipitation during an El Niño event.

2C30A shows a similar pattern of the future change daily precipitation as 2C20 (Fig. 15c). In most areas the magnitudes of the changes are comparable, in others such as over the western tropical Pacific Ocean they differ. As indicated in the nonlinear component of the change in 2C30A, the increase in precipitation is particularly strong over the western tropical Pacific Ocean and Indonesia with anomalies exceeding 1.5 mm/day (Fig. 15e). Over the central and eastern part of the tropical Pacific Ocean, on the other hand, the future increase in daily precipitation is markedly reduced. These anomalies are accounted for by the fact that the marked El Niño like warming pattern in the tropical Pacific Ocean has not emerged in 2C30A because of the considerably weaker global warming associated with the direct effect and the first indirect of sulphate aerosols (see Fig. 13c). The second indirect effect of sulphate aerosols is caused by more but smaller cloud droplets that reduce the precipitation efficiency and therefore enhance the cloud lifetime and, hence, the cloud reflectivity (Albrecht 1989). The consideration of this effect in the cloud parameterization scheme of the ECHAM5 AGCM would, therefore, alter the simulated effect of the higher aerosol load in 2C30A by reducing (enhancing) the future increase (reduction) in precipitation in those areas where sulphate aerosols are produced, i.e., the industrialized areas in the Northern Hemisphere and the subtropics. In addition, the consideration of other kinds of aerosols, i.e., organic and black carbon as well as mineral dust and sea salt, could alter the simulated changes in precipitation. This is because the global hydrological sensitivity is about three times larger for aerosol forcing than for greenhouse gas forcing (Feichter et al. 2004). Roeckner et al. (2006) actually found a considerable reduction in daily precipitation in many parts of the globe as a consequence of enhanced carbonaceous aerosol burdens, particularly at low latitudes, where also the main sources of these kinds of aerosols are located.

5.5 Sea-level pressure

For the future, A1B shows a pronounced reduction of the sea-level pressure at high latitudes in both hemispheres and an increase at mid-latitudes (Fig. 16a). In the tropics, the atmospheric pressure is reduced in one half of the globe, reaching from the eastern Pacific Ocean over South America, the Atlantic Ocean and Africa into the western Indian Ocean, and enhanced in the other half. In the Southern Hemisphere mid-latitudes, these changes indicate a southward shift of the predominant ridge-trough system, with ridges located west of South America over the South Pacific Ocean, between South America and Africa over the

South Atlantic Ocean and between Africa and Australia over the South Indian Ocean. In the Northern Hemisphere, on the other hand, the changes indicate an intensification of both the Aleutian Low over the North Pacific Ocean and the Icelandic Low over the North Atlantic Ocean. In the Atlantic/European sector also the Azores High is intensified in the future, leading to a strengthening of the North Atlantic Oscillation. The reduction of the atmospheric pressure over the eastern tropical Pacific Ocean and the increase over the western part indicate an intensification of the Southern Oscillation in response to the El Niño like warming pattern (e.g., Trenberth and Shea 1987; see Fig. 13a). The reduction of the sea-level pressure at high latitudes and an increase at lower mid-latitudes is a dynamical response to the changes in the meridional temperature gradient (e.g., Räisänen 2001). In the Southern Hemisphere, for instance, the reduction of the sea-level pressure at high latitudes and the increase at mid-latitudes was found to be related to a southward shift of the strongest westerly winds in the troposphere forced by changes in the meridional temperature gradient (Kushner et al. 2001). Räisänen (1998) identified changes in the vertically integrated meridional momentum flux convergence by high-frequency transient eddies as an important forcing mechanism for the aforementioned changes in sea-level pressure in both hemispheres.

2C20 gives the same general structure of the future changes in the sea-level pressure with a decrease in the tropics and at high latitudes and an increase at mid-latitudes but with smaller magnitudes than A1B (Fig. 16b). The main differences with A1B are the relatively weak reduction of the sea-level pressure in the Antarctic region accompanied by a weaker increase at Southern Hemisphere mid-latitudes and a relatively strong reduction over the Barents and the Kara Sea accompanied by a stronger intensification of the Azores high (Fig. 16d). The differences in the Southern Hemisphere are the dynamical response to the less pronounced strengthening of the meridional temperature gradient in 2C20 (see Fig. 13d). The differences over the Barents Sea and the Kara Sea, on the other hand, are the dynamical response to the relatively strong increase of the meridional temperature gradient in this particular region. In the tropics, except for the Indian Ocean basin, the nonlinear component of the change in 2C20 manifest the negative phase of the Southern Oscillation, due to the fact that the El Niño like warming pattern is not pronounced in 2C20.

2C30A, on the other hand, shows a relatively strong reduction of the sea-level pressure in the Arctic region (Fig. 16c, e) despite the somewhat weaker global warming than 2C20 and 2C30, typically leading to a weaker enhancement of the meridional pressure gradient. Apparently, long-term internal variability in the coupled climate

Sea-level pressure

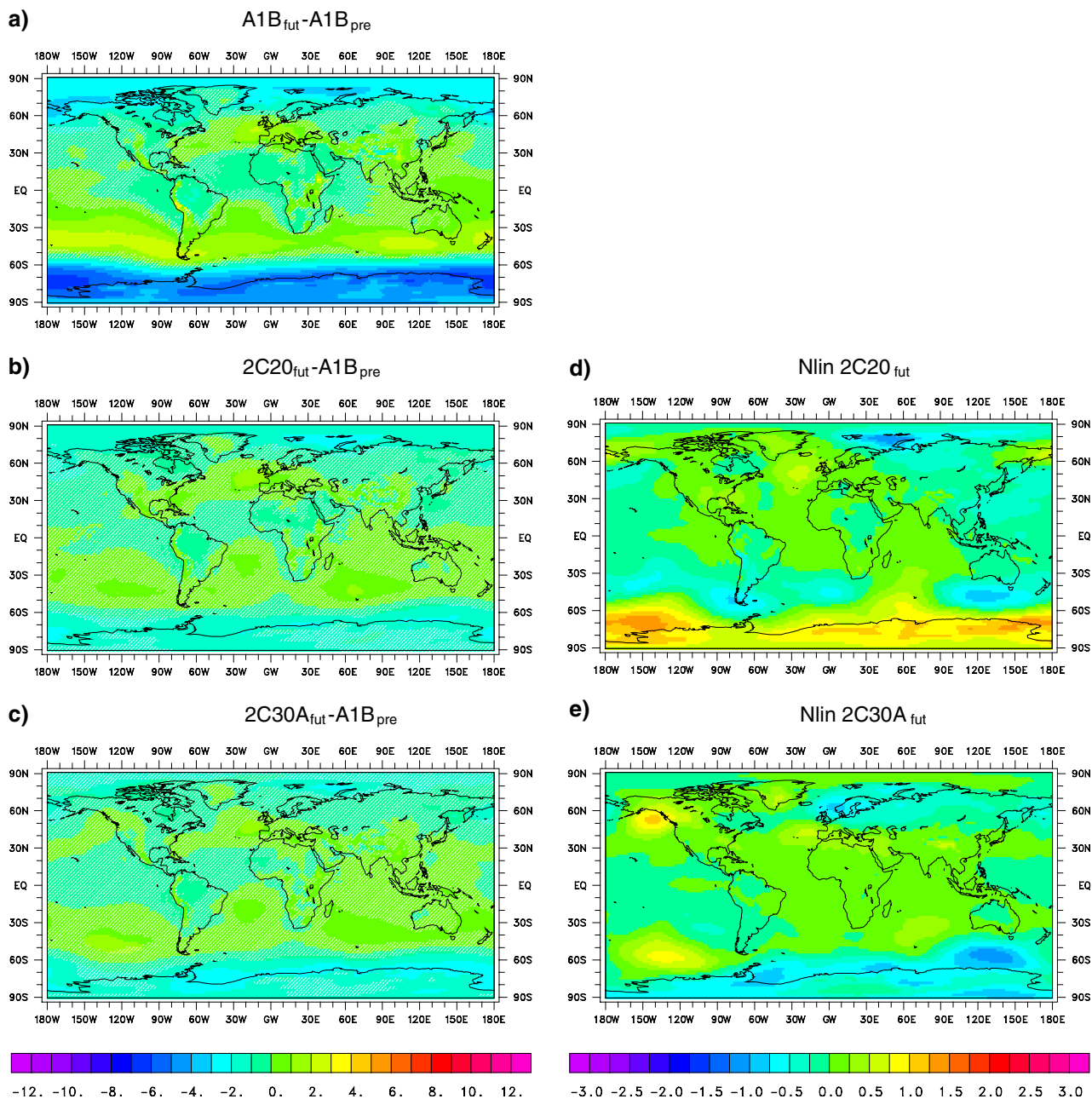


Fig. 16 As Fig. 13, but for mean sea-level pressure. The significance level is at 97.5% (a–c). Units are hPa, the contour interval is 1 hPa (a–c) and 0.25 hPa (d, e)

system can overrule the effect of the anthropogenic climate forcing. The positive anomalies over the South Pacific Ocean as well as the negative ones over the Wedell Sea and south of Australia are due to the relative weak warming over the Amundsen Sea and the relatively strong warming over the Wedell Sea and south of Australia, respectively (see Fig. 13e). In the Atlantic/European sector the North Atlantic Oscillation is further enhanced, as indicated by the negative anomalies over northern Europe the positive ones

further south as a response to the amplified meridional temperature gradient in this region.

6 Summary and conclusions

In this study, concentrations of the well-mixed greenhouse gases, the stratospheric ozone concentration as well as the anthropogenic sulphate aerosol load are prescribed to the

ECHAM5/MPI-OM coupled climate model so that the simulated global warming does not exceed 2°C relative to pre-industrial times. The simulated climatic changes in various meteorological and oceanic variables associated with this so-called “2°C-stabilization” scenario are presented and compared to the respective changes associated with the SRES A1B scenario. The A1B scenario is one of the three SRES emission scenarios chosen for the AR4, for which alternative developments of energy are balanced with those based on fossil fuels. The climatic changes due to the relatively weak climate forcing as the one associated with the 2°C-stabilization scenario supplement AR4 in that such a stabilization scenario can only be achieved by mitigation activities, which have not been considered in any of the SRES scenarios. Also, the impact of the anthropogenic sulphate aerosol load and stratospheric ozone concentrations on the simulated climatic changes is investigated.

For the ECHAM5/MPI-OM coupled climate model, the 2°C-stabilization scenario is characterized by the following atmospheric concentrations of the well-mixed greenhouse gases: 418 ppm (CO₂), 2,026 ppb (CH₄), 331 ppb (N₂O), 786 ppt (CFC-11), and 486 ppt (CFC-12). These greenhouse gas concentrations correspond to those for 2020 according to the SRES A1B scenario (Nakićenović et al. 2000). At the same time, the anthropogenic sulphate aerosol load and the stratospheric ozone concentrations are changed to the level in 2100, again according to the SRES A1B scenario. The anthropogenic sulphate aerosol load is reduced to from 1.00 TgS in 2020 to 0.23 TgS in 2100 for the global annual mean, while the stratospheric ozone concentrations are enhanced in the upper stratosphere at high latitudes, i.e., by about 300 ppb in the Southern and about 140 ppb in the Northern Hemisphere.

The future changes in climate associated with the 2°C-stabilization scenario show many of the typical features of other climate change scenarios, including those associated with stronger climatic forcings. That are a pronounced warming, particularly at high latitudes accompanied by a marked reduction of the sea-ice cover, a substantial increase in precipitation in the tropics as well as at mid- and high latitudes in both hemispheres but a marked reduction in the subtropics, a significant strengthening of the meridional temperature gradient between the tropical upper troposphere and the lower stratosphere in the extratropics accompanied by a pronounced intensification of the westerly winds in the lower stratosphere, and a strengthening of the westerly winds in the Southern Hemisphere extratropics throughout the troposphere. The magnitudes of these changes, however, are somewhat weaker than for the scenarios associated with stronger global warming due to stronger climatic forcings, such as the SRES A1B scenario. Some of the climatic changes associated with the 2°C-

stabilization are relatively strong with regard to the magnitude of the simulated global warming, i.e., the pronounced warming and sea-ice reduction in the Arctic region, the strengthening of the meridional temperature gradient at the northern high latitudes and the general increase in precipitation. Other climatic changes, i.e., the El Niño like warming pattern in the tropical Pacific Ocean and the corresponding changes in the distribution of precipitation in the tropics and in the Southern Oscillation, are not as markedly pronounced as for the scenarios with a stronger global warming. The 2°C stabilization scenario gives a warming well below 2.7°C in the area around Greenland during summer. Only near the northeastern edge of Greenland this threshold, at which the Greenland ice-sheet is expected to start melting (Gregory et al. 2004a, b), is actually reached. This indicates that a stabilization of the global mean temperature change at 2°C would, indeed, avoid this kind of “dangerous climate change” (Schellnhuber et al. 2006) almost completely.

A higher anthropogenic sulphate aerosol load (for 2030 as compared to the level in 2100 according to the SRES A1B scenario) generally weakens the future changes in climate, particularly for precipitation. The most pronounced effects occur in the Northern Hemisphere and in the tropics, where also the main sources of anthropogenic sulphate aerosols are located. Because of the effects of different kinds of aerosols, with negative radiative effects for sulphate and organic carbon and positive radiative effects for black carbon, the changes in the aerosol load have an important effect on magnitude of the global warming associated with certain concentrations of the well-mixed greenhouse gases. Hence, changes in the aerosol load have to be considered in strategies aiming to keep the future global warming below 2°C.

The idealized case of keeping the concentrations of the well-mixed greenhouse gases constant at a certain point in time, which is chosen in this study, requires that the emission rates of these forcing agents are balanced by the rates at which these constituents are removed from the atmosphere. Given the different residence times of the various greenhouse gases, i.e., 12 ± 3 years for CH₄, 120 years for N₂O, 45 years for CFC-11, 100 years for CFC-12 and the potentially very long residence time for CO₂ (e.g., Solomon et al. 2007), a more realistic case would be continuing slight increases in the concentrations of CO₂ and N₂O for at least a century and a peaking concentration of CH₄ after a few decades and a subsequent reduction, in line with the so-called Alternative scenario proposed by Hansen and Sato (2004).

Obviously, the magnitude of the allowable greenhouse gas concentrations at which the future warming does not exceed the threshold of 2°C depends on the climate sensitivity of the coupled climate model. A climate model with a

higher sensitivity would require weaker greenhouse gas concentrations and a model with a lower sensitivity would allow for higher concentrations and, hence, for a later time at which the greenhouse gas concentrations have to be kept constant. Another source of uncertainty is the consideration of the various effects of different kinds of aerosols in the climate model. ECHAM5/MPI-OM does, for instance, not include the second indirect effect of sulphate aerosols. Moreover, other kinds of aerosols such as organic and black carbon as well as mineral dust and sea salt are not considered in the simulations used here. The consideration of these effects would influence the magnitude of the global warming. The second indirect effect of sulphate aerosols and the consideration of organic carbon aerosols lead to a weaker global warming, while the consideration of black carbon aerosols leads to a stronger global warming. The consideration of these effects would also affect the regional changes in climate. Black carbon aerosols, for instance, amplify the warming at high latitudes because of the albedo effect of black carbon deposited on snow and, hence, the melting of the sea-ice. The second indirect effect of sulphate aerosols, on the other hand, reduces the precipitation efficiency and, hence, future increases in precipitation.

Acknowledgments This work was supported by the Danish Environmental Protection Agency under contract no. M4049-0053 and the European Commission through the ENSEMBLES project under contract no. GOCE-CT-2003-505539. I thank one of the anonymous reviewers for very helpful comments and suggestions that helped to improve the manuscript.

References

- ACIA (2005) Arctic climate impact assessment. Cambridge University Press, Cambridge, pp 1042
- Albrecht B (1989) Aerosols, cloud microphysics, and fractional cloudiness. *Science* 245:1227–1230
- Archer D, Martin P, Buffett B, Brovkin V, Rahmsdorf S, Ganopolski A (2004) The importance of ocean temperature to biogeochemistry. *Earth Planet Sci Lett* 222:333–348
- Arzel O, Fichefet T, Goosse H (2006) Sea ice evolution over the 20th and 21st centuries as simulated by current AOGCMs. *Ocean Model* 12:401–415
- Boucher O, Lohmann U (1995) The sulphate-CCN-cloud albedo effect: a sensitivity study using two general circulation models. *Tellus* 47B:281–300
- Boucher O, Pham M, Venkataraman C (2002) Simulation of the atmospheric sulfur cycle in the Laboratoire de Météorologie Dynamique general circulation model. Model description, model evaluation, and global and European budgets. *IPSL scientific note* 23, pp 26
- Brasseur GP, Roeckner E (2005) Impact of improved air quality on the future evolution of climate. *Geophys Res Lett* 32. doi: [10.1029/2005GL023902](https://doi.org/10.1029/2005GL023902)
- Buffett B, Archer D (2004) Global inventory of methane clathrate: sensitivity to changes in the deep ocean. *Earth Planet Sci Lett* 227:185–199
- Collins WD, 20 co-authors (2006) Radiative forcing by well-mixed greenhouse gases: estimates from climate models in the Intergovernmental Panel on Climate Change (IPCC) Fourth Assessment Report (AR4). *J Geophys Res* 111. doi: [10.1029/2005JD006713](https://doi.org/10.1029/2005JD006713)
- Den Elzen M, Meinshausen M (2006) Multi-gas emission pathways for meeting the EU 2°C climate target. In: Schellnhuber HJ, Cramer W, Nakićenović NJ, Wigley T, Yohe G (eds) *Avoiding dangerous climate change*. Cambridge University Press, Cambridge, pp 299–309
- Feichter J, Roeckner E, Lohmann U, Liepert B (2004) Nonlinear aspects of the climate response to greenhouse gas and aerosol forcing. *J Clim* 17:2384–2398
- Flato GM, Participating CMIP Modelling Groups (2004) Sea-ice and its response to CO₂ forcing as simulated by global climate models. *Clim Dyn* 23:229–241
- Forster PM, Taylor KE (2006) Climate forcings and climate sensitivities diagnosed from coupled climate simulations. *J Clim* 19:6181–6194
- Forster PM, 14 co-authors (2007) Changes in atmospheric constituents and in radiative forcing. In: Solomon S, Qin D, Manning M, Chen Z, Marquis M, Averyt KB, Tignor M, Miller HL (eds) *Climate change 2007: the physical science basis*. Cambridge University Press, Cambridge, pp 129–234
- Friedlingstein P, Dufresne JJ, Cox PM, Rayner P (2003) How positive is the feedback between climate change and the carbon cycle? *Tellus* 55B:692–700
- Giorgi F (2005) Interdecadal variability of regional climate change: implications for the development of regional climate scenarios. *Meteorol Atmos Phys* 89:1–15
- Giorgi F (2006) Climate change hot-spots. *Geophys Res Lett* 33. doi: [10.1029/2006GL025734](https://doi.org/10.1029/2006GL025734)
- Gregory JM, Ingram WJ, Palmer MA, Jones GS, Stott PA, Thorpe RB, Lowe JA, Johns TC, Williams KD (2004a) A new method for diagnosing radiative forcing and climate sensitivity. *Geophys Res Lett* 31. doi: [10.1029/2003GL018747](https://doi.org/10.1029/2003GL018747)
- Gregory JM, Huybrechts P, Raper SCB (2004b) Threatened loss of the Greenland ice-sheet. *Nature* 428:616
- Hansen J, Sato M (2004) Greenhouse gas growth rates. *Proc Natl Acad Sci* 101:16109–16114
- Hansen J, 46 co-authors (2007) Dangerous human-made interference with climate: a GISS modelE study. *Atmos Chem Phys* 7:2287–2312
- Hess M, Koepke P, Schult I (1998) Optical properties of aerosols and clouds: the software package OPAC. *Bull Amer Meteor Soc* 79:831–844
- Huybrechts P, Letreguilly A, Reeh A (1991) The Greenland ice-sheet and global warming. *Glob Planet Change* 89:399–412
- Johannessen OM, 11 co-authors (2004) Arctic climate change: observed and modelled temperature and sea-ice variability. *Tellus* 56A:328–341
- Jones CD, Cox P, Essery RLH, Roberts DL, Woodage MJ (2003a) Strong carbon cycle feedbacks in a climate model with interactive CO₂ and sulphate aerosols. *Geophys Res Lett* 30:1479–1483
- Jones CD, Cox P, Huntingford C (2003b) Uncertainty in climate-carbon-cycle projections associated with the sensitivity of soil respiration to temperature. *Tellus* 55B:642–648
- Jungclaus JH, Botzet M, Haak H, Keenlyside N, Luo JJ, Latif M, Marotzke J, Mikolajewicz U, Roeckner E (2006) Ocean circulation and tropical variability in the coupled model ECHAM5/MPI-OM. *J Clim* 19:3952–3972
- Kiehl JT, Schneider TL, Portman RW, Solomon S (1999) Climate forcing due to tropospheric and stratospheric ozone. *J Geophys Res* 104:31239–31254

- Knutti R, Meehl GA, Allen MR, Stainforth DA (2006) Constraining climate sensitivity from the seasonal cycle in surface temperature. *J Clim* 19:4224–4233
- Kushner PJ, Held IM, Delworth TL (2001) Southern Hemisphere atmospheric circulation response to global warming. *J Clim* 14:2238–2249
- Lohmann U, Feichter J (2005) Global indirect aerosol effects: a review. *Atmos Chem Phys* 5:715–737
- Marsland SJ, Haak H, Jungclaus JH, Latif M, Röske F (2003) The Max-Planck-Institute global ocean/sea ice model with orthogonal curvilinear coordinates. *Ocean Model* 5:91–127
- Meehl GA, Washington WM, Collins WD, Arblaster JM, Hu A, Buja LE, Strand WG, Teng H (2005) How much more global warming and sea level rise? *Science* 307:1769–1772
- Meehl GA, 13 co-authors (2007) Global climate projections. In: Solomon S, Qin D, Manning M, Chen Z, Marquis M, Averyt KB, Tignor M, Miller HL (eds) *Climate change 2007: the physical science basis*. Cambridge University Press, Cambridge, pp 747–845
- Meinshausen M (2006) What does a 2°C target mean for greenhouse gas concentrations? A brief analysis based on multi-gas emission pathways and several climate sensitivity uncertainty estimates. In: Schellnhuber HJ, Cramer W, Nakićenović NJ, Wigley T, Yohe G (eds) *Avoiding dangerous climate change*. Cambridge University Press, Cambridge, pp 265–279
- Mitchell TD (2003) Pattern scaling. An examination of the accuracy of the technique of describing future climates. *Clim Change* 60:217–242
- Mitchell JFB, Johns TC, Eagles M, Ingram WJ, Davis RA (1999) Towards the construction of climate change scenarios. *Clim Change* 41:547–581
- Murphy JM, Sexton DMH, Barnett DN, Jones GS, Webb MJ, Collins M, Stainforth DA (2004) Quantification of modelling uncertainties in a large ensemble of climate change simulations. *Nature* 430:768–772
- Nakićenović NJ, 27 co-authors (2000) *IPCC special report on emission scenarios*. Cambridge University Press, Cambridge, pp 599
- Pham M, Boucher O, Hauglustaine D (2005) Changes in atmospheric sulphur burdens and concentrations and resulting radiative forcings under IPCC SRES emission scenarios for 1990–2100. *J Geophys Res* 110. doi:10.1029/2004JD005125
- Piani C, Frame DJ, Stainforth DA, Allen MR (2005) Constraints on climate change from a multi-thousand member ensemble of simulations. *Geophys Res Lett* 32. doi:10.1029/2005GL024452
- Räisänen J (1998) CO₂- and aerosol-induced changes in vertically integrated zonal momentum budget in a GCM experiment. *J Clim* 11:625–639
- Räisänen J (2001) CO₂-induced climate change in CMIP2 experiments: quantification of agreement and role of internal variability. *J Clim* 14:2088–2104
- Räisänen J, Hansson U, Ullerstig A, Döscher R, Graham LP, Jones C, Meier HEM, Samuelson P, Willén U (2004) European climate in the late twenty-first century: regional simulations with two driving global models and two forcing scenarios. *Clim Dyn* 22:13–31
- Ramaswamy V, 8 co-authors (2001) Radiative forcing of climate change. In: Houghton JT, Ding Y, Griggs DJ, Noguer M, van der Linden PJ, Dai X, Maskell K, Johnson CS (eds) *Climate Change 2001. The scientific basis*. Cambridge University Press, Cambridge, pp 349–416
- Roeckner E, Bengtsson L, Feichter J, Lelieveld J, Rodhe H (1999) Transient climate change simulations with a coupled atmosphere-ocean CGM including the tropospheric sulfur cycle. *J Clim* 12:3004–3032
- Roeckner E, 13 co-authors (2003) The atmospheric general circulation model ECHAM5. Part I: Model description. MPI-Report 349, pp 127
- Roeckner E, Brokopf R, Esch M, Giorgetta M, Hagemann S, Kornblüh L, Manzini E, Schlese U, Schulzweida U (2006) Sensitivity of simulated climate to horizontal and vertical resolution in the ECHAM5 atmosphere model. *J Clim* 19:3771–3791
- Rotstayn LD, Penner JE (2001) Indirect aerosol forcing, quasi-forcing and climate response. *J Clim* 14:2960–2975
- Schellnhuber HJ, Cramer W, Nakićenović NJ, Wigley T, Yohe G (eds) (2006) *Avoiding dangerous climate change*. Cambridge University Press, Cambridge, pp 392
- Schulz M, 22 co-authors (2006) Radiative forcing by aerosols as derived from the AeroCom present-day and pre-industrial simulations. *Atmos Chem Phys* 6:5225–5246
- Smith JB, Schellnhuber HJ, Mirza MQM (2001) Vulnerability to climate change and reasons for concern: a synthesis. In: McCarthy JJ, Canziani OF, Leary NA, Dokken DJ, White KS (eds) *Climate change 2001. Impacts, adaptation, and vulnerability*. Cambridge University Press, Cambridge, pp 913–967
- Solomon S, Qin D, Manning M, Chen Z, Marquis M, Averyt KB, Tignor M, Miller HL (eds) (2007) *Climate change 2007: the physical science basis*. Cambridge University Press, Cambridge, pp 996
- Trenberth KE, Shea DJ (1987) On the evolution of the Southern Oscillation. *Mon Weather Rev* 112:326–332
- Trenberth KE, Caron JM, Stepniak DP, Worley S (2002) Evolution of El Niño-Southern Oscillation and global atmospheric surface temperatures. *J Geophys Res* 107. doi:10.1029/2000JD000298
- Twomey SA (1977) The influence of pollution on the shortwave albedo of clouds. *J Atmos Sci* 34:1149–1152
- United Nations (1992) *United Nations Framework Convention on Climate Change (UNFCCC)*. Available at <http://www.unfccc.int>
- Wigley TML, Raper SCB (2001) Interpretation of high projections for global-mean warming. *Science* 293:451–454
- Yamaguchi K, Noda A (2006) Global warming patterns over the North Pacific: ENSO versus AO. *J Meteorol Soc Jpn* 84:221–241